Developmental Biology

Motor neurons are dispensable for the assembly of a sensorimotor circuit for gaze stabilization

Reviewed Preprint

Published from the original preprint after peer review and assessment by eLife.

About eLife's process

Reviewed preprint version 1
April 22, 2024 (this version)

Sent for peer review
March 8, 2024

Posted to preprint server
January 27, 2024

Dena Goldblatt, Başak Rosti, Kyla R. Hamling, Paige Leary, Harsh Panchal, Marlyn Li, Hannah Gelnaw, Stephanie Huang, Cheryl Quainoo, David Schoppik

Depts. of Otolaryngology, Neuroscience & Physiology, and the Neuroscience Institute, NYU Langone Health • Center for Neural Science, New York University

Abstract

Sensorimotor reflex circuits engage distinct neuronal subtypes, defined by precise connectivity, to transform sensation into compensatory behavior. Whether and how motor neuron populations specify the subtype fate and/or sensory connectivity of their pre-motor partners remains controversial. Here, we discovered that motor neurons are dispensable for proper connectivity in the vestibular reflex circuit that stabilizes gaze. We first measured activity following vestibular sensation in premotor projection neurons after constitutive loss of their extraocular motor neuron partners. We observed normal responses and topography indicative of unchanged functional connectivity between sensory neurons and projection neurons. Next, we show that projection neurons remain anatomically and molecularly poised to connect appropriately with their downstream partners. Lastly, we show that the transcriptional signatures that typify projection neurons develop independently of motor partners. Our findings comprehensively overturn a long-standing model: that connectivity in the circuit for gaze stabilization is retrogradely determined by motor partner-derived signals. By defining the contribution of motor neurons to specification of an archetypal sensorimotor circuit, our work speaks to comparable processes in the spinal cord and advances our understanding of general principles of neural development.

eLife assessment

This **important** study asks whether motor neurons within the vestibulo-ocular circuit of zebrafish are required to determine the identity, connectivity, and function of upstream premotor neurons. They provide **convincing** genetic, anatomical and behavioral evidence that the answer is no. This work is of general interest to developmental neurobiologists and motivates future studies of whether motor neurons are dispensable for assembly of other sensorimotor neural circuits.

Introduction

Developing sensorimotor reflex circuits must precisely connect functional subtypes of neurons to ensure appropriate behavior. For example, withdrawal from noxious stimuli requires maturation of a sensorimotor circuit that uses subtypes of spinal interneurons to transform noxious stimulation into activation of both ipsilateral flexor and contralateral extensor motor neurons [1]. Work over the past 40 years has highlighted motor partner populations as possible orchestrators of connectivity in pre-motor reflex circuits [2–6], but controversy remains about the nature of their role. In the spinal cord, molecular perturbations of motor neuron identity have provided evidence both for [7–11] and against [12–16] an instructive role in determining pre-motor fate. Part of this controversy stems from the wide variety of inputs to spinal motor neurons [17], the molecular and functional heterogeneity of pre-motor interneurons [14,15], and their complex roles in gait and posture [18]. Further, transcription factors play multivariate and redundant roles in spinal motor neuron development [19,20], such that the effects of molecular perturbations of identity can be masked.

The sensorimotor circuit for vertical gaze stabilization offers a simple framework to evaluate whether and how motor neurons shape pre-motor circuit fate and connectivity. The vertebrate vestibulo-ocular reflex circuit consists of three neuron types – peripheral sensory, central projection, and extraocular motor neurons – that stabilize gaze after head/body tilts (**Figure 1A**) [21]. Subtype fate, anatomical connectivity, and function are inextricably linked: directionally-tuned sensory neurons innervate nose-up/nose-down subtypes of projection neurons, which in turn innervate specific motor neurons that selectively control either eyes-down or eyes-up muscles [3,22–29]. As both the recipients and origin of directional information, projection neuron fate specification is tantamount to proper circuit assembly. Recent work has established the vertical vestibulo-ocular reflex circuit in zebrafish as a model to uncover determinants of fate and connectivity [24–26,29] given the ease of optical imaging, abundant tools for genetic perturbations, rapid development, and robust evolutionary conservation.

The current model for vestibulo-ocular reflex circuit development was motivated by pioneering work in chick [3,30] and formalized by Hans Straka: “[circuit assembly] is accomplished by a specification process that retrogradely transmits post-synaptic target identities to pre-synaptic neurons.” [31]. In its strongest form, this “retrograde” model posits a causal role for extraocular motor neurons in specifying the fate (sensory selectivity) of central projection neurons. This key prediction – that loss of motor neurons would disrupt sensory selectivity in pre-synaptic projection neurons – remains untested. In zebrafish, extraocular motor neurons are temporally poised for such a role. Motor neurons are organized into spatial pools, and though synaptogenesis at ocular muscle targets begins late in development [32], motor neuron fate (muscle target and pool location) is determined early [33]. Projection neurons are born at roughly the same time as motor neurons and extend axons shortly afterwards, poising them to receive deterministic signals that could retrogradely specify their sensory selectivity [29].

Here, we adopted a loss-of-function approach to determine whether motor partner populations specify identity or instruct connectivity across an entire vestibular reflex circuit in zebrafish. We generated a new mutant allele for the *phox2a* gene to eliminate the extraocular motor neurons used for vertical gaze stabilization. Combining functional, anatomical, and sequencing approaches, we then demonstrated that motor neurons are dispensable for three aspects of pre-motor reflex circuit assembly: (i) directionally-appropriate connectivity between sensory and projection neurons, (ii) assembly of projection neurons with motor partners, and (iii) the transcriptional profiles of projection neurons. The current model of vestibulo-ocular reflex circuit development must therefore be revised: up/down projection neuron subtype fate cannot be

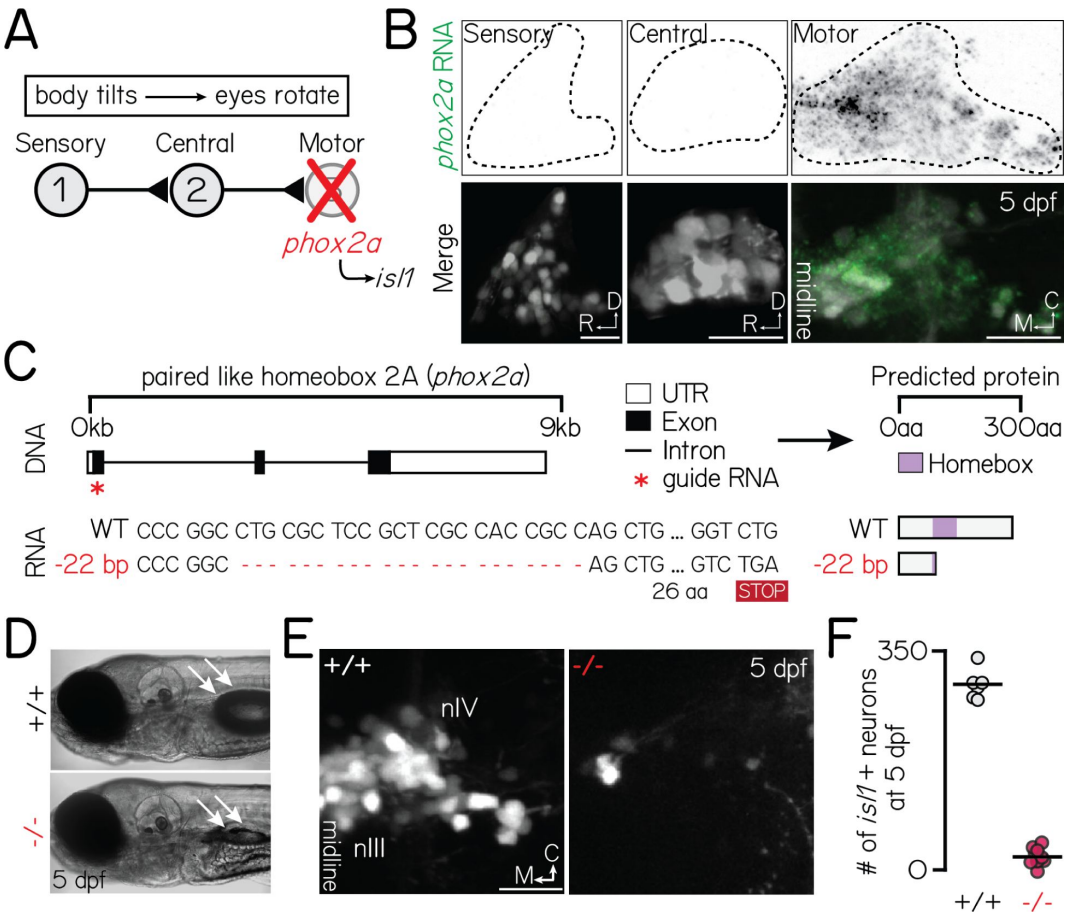

Figure 1

phox2a loss-of-function mutants fail to develop nIII/nIV motor neurons and vertical eye rotation behavior.

Associated with **Figure S1**.

(A) Schematic of vestibulo-ocular reflex circuitry and the genetic loss-of-function approach used to perturb motor-derived signals.

(B) Fluorescent *in situ* hybridization showing *phox2a* transcript expression in statoacoustic ganglion sensory afferents (left), central projection neurons in the tangential nucleus (middle), or nIII/nIV extraocular motor neurons (right) at 5 days post-fertilization (dpf). Top: probe only, nuclei outlined with dashed lines. Bottom: probe (green) merged with somata, labeled by *Tg(-6.7Tru.Hcrtr2:GAL4-VP16);Tg(UAS-E1b:Kaede)* (sensory, central) or *Tg(isl1:GFP)* (motor).

(C) Schematic of CRISPR/Cas9 mutagenesis approach. Top: Red star shows location of guides against *phox2a* DNA. Bottom: RNA sequence in wildtype and *phox2a*^{d22} alleles. Red dashed lines show deleted sequence; "STOP" box shows predicted premature stop codon due to deletion. Right shows predicted protein sequence.

(D) Transmitted light image of a 5 dpf wildtype (top) and *phox2a* null mutant (bottom). White arrows point to a normally inflated (top) or absent (bottom) swim bladder.

(E) Images of nIII/nIV motor neurons in one hemisphere, labeled by *Tg(isl1:GFP)*, in wildtype siblings (left) and *phox2a* null mutants (right) at 5 dpf. Scale bar, 20 μm.

(F) Quantification of the number of *Tg(isl1:GFP)*+ neurons in nIII/nIV from N=6 wildtype siblings and N=10 *phox2a* null mutants.

retrogradely established by a motor partner-derived signal. Instead, the signals that specify fate must lie elsewhere. More broadly, our work argues against a deterministic role of motor neurons in specifying the fate and sensory connectivity of pre-motor circuit components.

Results

Constitutive loss of *phox2a* prevents extraocular motor neuron specification and impairs vertical gaze stabilization behavior

Extraocular motor neurons for vertical/torsional gaze stabilization are located in cranial nuclei III (nIII) and IV (nIV). To eliminate nIII/nIV motor neurons and by extension, any secreted signals, we used a genetic loss-of-function approach (**Figure 1A**). A single highly-conserved transcription factor, *phoxa*, specifies nIII/nIV fate [34–37]. In the vestibulo-ocular reflex circuit, *phox2a* is exclusively expressed in nIII/nIV motor neurons but not its upstream partners (**Figure 1B**). Therefore, *phox2a* is an ideal genetic target to eliminate motor-derived signals without compromising evaluations of upstream functional development. Prior mutagenesis established a *phox2a* loss-of-function allele in zebrafish [34], but the line has since been lost. Here, we generated three new *phox2a* loss-of-function alleles using CRISPR/Cas9 mutagenesis (**Figure 1C**) (one allele shown here; additional alleles described in Methods). Consistent with prior reports and human mutations [38], both eyes in *phox2a* null mutants were exotropic (rotated towards the ears) reflecting a loss of motor neurons in nIII/nIV. *phox2a* mutants failed to hatch from their chorions without manual intervention and did not inflate their swim bladders by 5 days post-fertilization (dpf) (**Figure 1D**), phenotypes not previously reported [34]. Consequently, null mutants do not survive past 7 dpf. We did not observe these morphological phenotypes in wildtype and heterozygous siblings (**Figure 1D**). As vestibulo-ocular reflex circuit architecture and behavior is established by 5 dpf [24,25,29], premature lethality did not preclude further measurements of circuit development.

To validate *phox2a* loss-of-function, we leveraged a downstream transcription factor: *isl1* [39]. The *Tg(isl1:GFP)* line [40] labels all nIII/nIV motor neurons except inferior oblique neurons [33], which comprise one of four pools for upwards eye rotations. We first quantified changes in the number of labeled nIII/nIV neurons (**Figure 1E**-**Figure 1F**). In *phox2a* mutants, we observed an expected and near-total loss of *isl1* expression (WT: 298±19 neurons across both hemispheres; null: 19±11 neurons; Wilcoxon rank sum test, $p=2.5\times10^{-4}$) at 5 dpf, well-after nIII/nIV differentiation is complete [33]. Unexpectedly, we also observed slightly fewer neurons in *phox2a* heterozygotes (heterozygote: 229±20 neurons; Wilcoxon rank sum test against WT, $p=6.7\times10^{-4}$). In heterozygotes, loss of *isl1* fluorescence was restricted to the medial domain of dorsal nIII, which contains some of the earliest-born neurons in nIII/nIV (**Figure S1A**-**Figure S1C**) [33]. Globally, this manifested as a rostral and ventral shift in the positions of all neurons mapped (**Figure S1D**) (two-sample, two-tailed KS test, WT vs. heterozygotes: mediolateral axis, p=0.13; rostrocaudal: $p=4.0\times10^{-29}$; dorsoventral: $p=2.5\times10^{-9}$). This region contains two motor pools that control the inferior (IR) and medial rectus (MR) muscles [33]. We conclude that *phox2a* acts in a dose- and birthdate-dependent manner to specify nIII motor pool fate.

Together, these observations validate our *phox2a* loss of function alleles as a selective means to disrupt nIII/nIV motor neuron fate specification and vertical eye rotation behavior.

Peripheral-to-central circuit assembly does not require motor partners

Vertical gaze stabilization requires that (1) peripheral VIIIth nerve sensory afferents relay tilt sensation (nose-up/nose-down) directly to projection neurons in the tangential nucleus, and (2) projection neurons innervate appropriate nIII/nIV pools (eyes-up/eyesdown). For proper circuit

function, appropriate connectivity must first develop across up/down circuit subtypes. The "retrograde" model predicts that motor partners specify circuit assembly. Therefore, in the absence of motor neurons, projection neurons should fail to respond selectively to directional tilt sensations – either due to loss of their fate, the fate of upstream sensory afferents, or sensory-to-central connectivity.

To evaluate upstream circuit formation, we measured tilt-evoked responses in projection neurons using Tilt-In-Place Microscopy (TIPM) [41] (**Figure 2A**-**Figure 2B**). Peripherally, tilts activate utricular VIIIth nerve sensory inputs to projection neurons [29,41]. We used a galvanometer to deliver tonic nose-up and nose-down pitch tilts to *phox2a* null larvae and sibling controls. We then measured the activity of a calcium indicator, GCaMP6s [42], in projection neurons. We performed experiments at 5 dpf, when nearly all projection neurons are selective for one tilt direction [29], circuit architecture is stable [25], and gaze stabilization behavior is directionally-appropriate [24].

Projection neuron responses and topography were strikingly unchanged in *phox2a* mutants compared to controls. We recorded the activity of n=297 neurons from N=16 *phox2a* mutants and n=440 neurons from N=21 sibling controls (Methods and **Table 1** split by genotype). We observed comparable ratios of projection neuron subtypes (sib: 46% nose-down, 47% nose-up, 7% untuned; *phox2a*: 49% nose-down, 44% nose-up, 7% untuned) (**Figure 2C**). Next, we evaluated their topography (**Figure 2D**-**Figure 2E**). Projection neurons are topographically organized along the dorso-ventral axis by their directional selectivity [29]. Global spatial separation between subtypes remained significant in *phox2a* mutants (one-way multivariate analysis of variance, p=0.004). We also compared the topography of nose-up and nose-down neurons separately across *phox2a* genotypes. Nose-down neurons were comparably distributed between null and control larvae (one-way multivariate analysis of variance, p=0.15). We observed a minor lateral shift to nose-up neurons in null mutants (median mediolateral position, sib: 15.2μm from medial edge; *phox2a*, 13.2μm; twotailed, two-sample KS test, $p=3.0\times10^{-4}$) but no changes in other spatial axes (dorsoventral: p=0.16; rostrocaudal: p=0.56). The small medial deviation (2μm across a 40μm space) is within the limits of our registration error. We conclude that projection neuron topography is established independently of motor partners.

Projection neuron sensitivity and selectivity also developed comparably between *phox2a* mutants and siblings (**Figure 2F**-**Figure 2K**). Projection neurons responded to tilt sensations with comparable magnitudes (**Figure 2G**-**Figure 2J**) (nose-down mean ΔFF, sib: 1.86±1.69; *phox2a*: 2.07±1.48; two-tailed Wilcoxon rank sum test, p=0.98; nose-up mean ΔFF, sib: 1.24±1.23; *phox2a*: 1.02±0.89; p=0.18). Previously, we defined a metric to describe a neuron's selectivity for one tilt direction (0 = equal responses to up/down; 1 = maximally selective) [29]. Directional selectivity remained unchanged in *phox2a* mutants (**Figure 2H**-**Figure 2K**) (nose-down mean index, sib: 0.73±0.29; *phox2a*: 0.68±0.29; two-tailed Wilcoxon rank sum test, p=0.85; nose-up mean index, sib: 0.85±0.26; *phox2a*: 0.81±0.29; p=0.12). Collectively, this demonstrates that the functional responses of projection neurons and, by inference, connectivity with utricular afferents are not shaped by motor partners.

Ventral projection neurons receive additional input from the semicircular canals [29], which encode phasic (fast) tilt sensation. To activate sensory afferents from the semicircular canals, we used TIPM to deliver two impulses of angular rotation (**Figure 3A**-**Figure 3B**) [29,41]. We observed no changes in *phox2a* mutants. Projection neurons responded to impulses in comparable ratios (**Figure 3E**) (sib: 58% responsive; *phox2a*: 71% responsive). Responsive projection neurons remained localized to the ventral nucleus (dorsoventral axis: two-tailed, two-sample KS test, p=0.99). Lastly, the functional properties of projection neurons were unchanged (**Figure 3F**-**Figure 3G**). We observed no change in calcium response magnitudes (**Figure 3F**) (mean ΔFF, sib: 0.33±0.29; *phox2a*: 0.36±0.40; two-tailed Wilcoxon rank sum test, p=0.85) or lack of directional

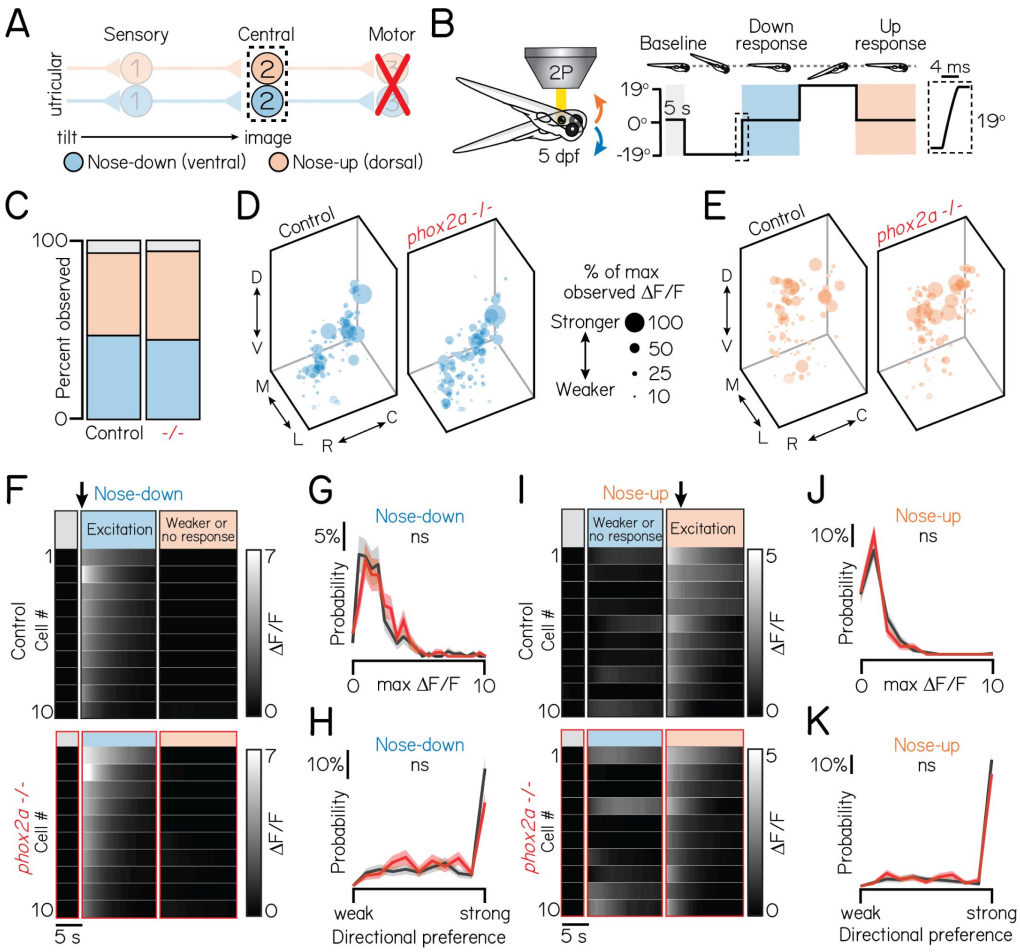

Figure 2

Motor neurons are dispensable for proper connectivity between utricular sensory afferents and projection neurons.

Associated with **Table 1**.

(A) Schematic of pitch vestibulo-ocular reflex circuitry. Dashed lines outline projection neurons as calcium imaging target. Nose-down/eyes-up channel represented with blue; orange, nose-up/eyes-down.

(B) Schematic of tonic pitch-tilt stimulus delivered with Tilt-In-Place Microscopy (TIPM). Shaded regions show calcium imaging windows when fish were oriented horizontally immediately following tilts. Inset shows timecourse of the rapid step to restore horizontal position after tilts. Imaging experiments used larvae from the *Tg(isl1:GFP);Tg(-6.7Tru.Hcrtr2:GAL4-VP16);Tg(UAS:GCaMP6s)* line.

(C) Proportion of subtypes observed in sibling controls and *phox2a* null mutants. Blue: nose-down. Orange: nose-up. Grey: Neurons without directional tuning (criteria in Methods).

(D/E) Soma position of nose-down (blue) and nose-up (orange) neurons in sibling controls (left) and *phox2a* null mutants (right). Soma size scaled by strength of calcium response (ΔFF), normalized by max observed ΔFF.

(F/I) Heatmaps showing example tilt responses from nose-down (F) or nose-up (I) neurons in sibling controls (top) and *phox2a* null mutants (bottom). n=10 neurons with strongest ΔFF responses to tilts shown. Each row shows an individual neuron. Shaded bars show calcium imaging window immediately following restoration from eccentric position. Black arrow points to first second of tilt response used for analyses.

(G/J) Distributions of maximum ΔFF responses to tilts for nose-down (G) or nose-up (J) neurons in sibling controls (black) and *phox2a* null mutants (red). Solid and shaded lines show mean and standard deviation, respectively, of bootstrapped data (Methods)

(H/K) Distributions of directional tuning score to tilts for nose-down (H) or nose-up (K) neurons in sibling controls (black) and *phox2a* null mutants (red). Tuning score ranges from 0 (equal responses to both tilt directions, no tuning) to 1 (responses to one tilt direction only); criteria detailed in Methods. Solid and shaded lines show mean and standard deviation, respectively, of bootstrapped data.

	WT (all)	WT (sampled)	phox2a+/+	phox2a+/-	phox2a-/-	p val
Tonic tilt stimuli						
n (neurons/fish)	255/10	125/x	76/5	109/6	297/16	
% sampled (nose-up/nose-down/untuned)	50/44/7	37/54/9	40/54/7	56/37/7	44/50/6	
ΔFF, nose-up	1.28±1.23	1.27±1.19	1.09±1.03	1.12±0.90	1.02±0.82	0.26
ΔFF, nose-down	2.01±1.66	1.99±1.69	1.38±0.91	1.98±1.61	2.07±1.48	0.16
directional tuning strength, nose-up	0.84±0.28	0.83±0.30	0.87±0.26	0.81±0.28	0.81±0.29	0.70
directional tuning strength, nose-down	0.72±0.30	0.72±0.31	0.73±0.31	0.77±0.30	0.68±0.29	0.54
Impulse stimuli						
n (neurons/fish)	255/10	125/x	76/5	109/6	297/16	
% sampled (responsive/unresponsive)	58/42	57/43	57/43	60/39	70/30	
ΔFF	0.41±0.46	0.33±0.28	0.29±0.29	0.22±0.16	0.32±0.28	1.0E-05
directional tuning strength	0.08±0.36	0.10±0.38	0.003±0.41	0.07±0.48	0.07±0.41	0.64
Multiple comparisons	**genotype**		**p val**	**Cohen's d**		
ΔFF to impulses	WT to sampled		p=0.13	0.21		
	WT to +/+		p=0.04	0.27		
	WT to +/-		p=3.8E-06	0.48		
	WT to -/-		p=0.006	0.24		
	+/+ to +/-		p=0.47	0.34		
	+/+ to -/-		p=0.89	0.11		
	+/- to -/-		p=0.02	0.49		

Table 1

Statistical comparisons of tilt responses across genotypes.

WT (sampled) refers to an n=125 neuron subset, sampled with replacement from a reference dataset of wildtype projection neurons. Data shown is mean/standard deviation unless otherwise noted. p val generated from a one-way ANOVA with multiple comparisons. Associated with **Figure 2** and **Figure 3**.

selectivity (**Figure 3G**) (mean index, sib: 0.07±0.41; *phox2a*: 0.06±0.40; p=0.39). Therefore, fate and connectivity between phasic sensory afferents and projection neurons must not require motor partners.

Lastly, we considered whether loss of one subtype of nIII/nIV neurons might alter connectivity. For example, loss of eyes-down motor pools could impair wiring between their corresponding nose-up sensory and projection neuron partners. Here, we leveraged *phox2a* heterozygotes, which lack a subtype of nIII neurons (IR/MR) that contribute to downwards eye rotations (**Figure S1**). We observed no differences in tonic tilt responses between *phox2a* wildtype, heterozygote, and null larvae, though we did note a minor decrease in response strength to impulses (statistics in **Table 1**). We note that *phox2a* heterozygotes do not lack all motor pools for downwards eye rotations. Nevertheless, we conclude that individual motor pools do not meaningfully contribute to connectivity between sensory and projection neurons.

Taken together, these experiments demonstrate intact directional selectivity for two peripheral sensory inputs – utricular and semicircular canal VIIIth nerve afferents – and appropriate connectivity with projection neurons. We conclude that functional sensory-to-central circuit formation is established independently of motor partners.

Projection neurons remain competent to assemble with appropriate motor targets

Motor partners could secrete signals that initiate pre-motor axon outgrowth, target arriving axons to specific motor pools, or trigger synaptogenesis [3]. Motor pool topography in nIII/nIV reflects ocular muscle targets: dorsal pools innervate downward-rotating muscles (superior oblique and inferior rectus), while ventral pools target the converse (eyes-up, superior rectus and inferior oblique) [33,43]. In turn, projection neuron somatic and axonal organization mirrors motor pool topography [28,29], which could facilitate directionally-selective circuit assembly. We reasoned that projection neurons may fail to initiate axon outgrowth, target spatially-appropriate motor pools, and/or form synapses in *phox2a* mutants. To test this hypothesis, we measured changes in projection neuron anatomy at 5 dpf, when axonal arbors are established and stable [25].

To test whether projection neurons establish gross, long-range (hindbrain to midbrain) axonal outgrowths, we performed optical retrograde labeling [44] using a photolabile protein, Kaede. We targeted the medial longitudinal fasciculus at the midbrain-hindbrain boundary, which contains projection neuron axons [25,29] (**Figure 4A**). In both *phox2a* mutants and sibling controls, we observed retrograde photolabeling of projection neuron soma (**Figure 4B**), supporting that initial axon outgrowth does not require motor partner-derived signals.

Next, we evaluated whether projection neuron axons remain capable of wiring with spatially-appropriate motor partners. Projection neuron axons segregate along the dorsal (nose-up) and ventral (nose-down) axes according to their birth order (early/late born, respectively) [28,29] and the pool topography of their motor targets [33]. To test whether projection neurons retain this topography, we optically labeled the axons of early-born (before 30 hpf) projection neurons [29]. In *phox2a* mutants, axons remained dorsoventrally segregated at midbrain targets (**Figure 4C**, inset). Typically, projection neurons robustly collateralize to nIII/nIV targets at the midbrain-hindbrain boundary. We did not observe collaterals to nIII/nIV in *phox2a* mutants (**Figure 4C**). However, projection neurons still robustly arborized to more rostral, spinal-projecting targets in the nucleus of the medial longitudinal fasciculus, suggesting they retain the machinery necessary to collateralize. Consistent with this hypothesis, we observed that projection neurons formed occasional, small collaterals in *phox2a* mutants with few (1-5%) nIII/nIV neurons remaining (**Figure 4D**). We conclude that projection neurons remain competent to assemble with spatially-appropriate targets.

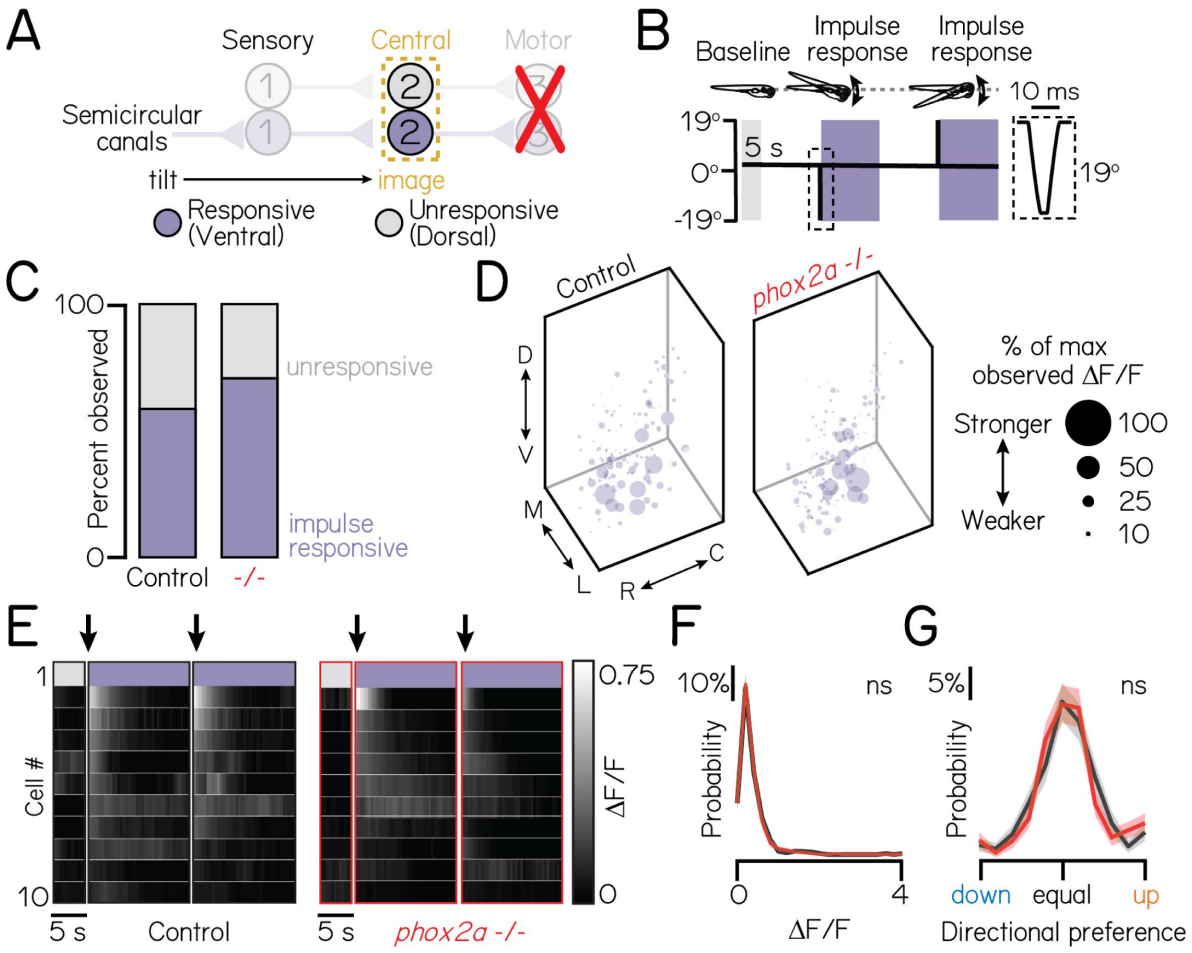

Figure 3

Motor neurons are dispensable for proper connectivity between semicircular canal sensory afferents and projection neurons.

Associated with **Table 1**.

(A) Schematic of impulse tilt experiments. Yellow dashed lines outline projection neurons as calcium imaging target. Impulse-responsive neurons (ventrally-localized) shown with purple; unresponsive neurons, grey.

(B) Schematic of impulse stimuli delivered with TIPM. Shaded regions show calcium imaging windows at horizontal immediately following impulses. Inset shows timecourse of impulse stimulus. Imaging experiments used larvae from the *Tg(isl1:GFP);Tg(-6.7Tru.Hcrtr2:GAL4-VP16);Tg(UAS:GCaMP6s)* line.

(C) Proportion of impulse-responsive (purple) and unresponsive (grey) neurons observed in sibling controls and *phox2a* null mutants.

(D) Soma position of impulse-responsive neurons in sibling controls (left) and *phox2a* null mutants (right). Soma size scaled by strength of calcium response (ΔFF), normalized by max observed ΔFF.

(E) Heatmaps showing example impulse responses from neurons in sibling controls (left) and *phox2a* null mutants (right). n=10 example neurons shown. Each row shows an individual neuron. Shaded bars show calcium imaging window immediately following impulse delivery. Black arrow points to first second of tilt response used for analyses. Note smaller scale (0-0.75) of impulse responses relative to **Figures 2F** and **2I**.

(F) Distributions of maximum ΔFF responses to impulses in sibling controls (black) and *phox2a* null mutants (red). Solid and shaded lines show mean and standard deviation, respectively, from bootstrapped data.

(G) Distributions of directional tuning score to impulses in sibling controls (black) and *phox2a* null mutants (red). Tuning score ranges from 0 (equal responses to both tilt directions, no tuning) to 1 (responses to one tilt direction only); criteria detailed in Methods. Solid and shaded lines show mean and standard deviation, respectively, from bootstrapped data.

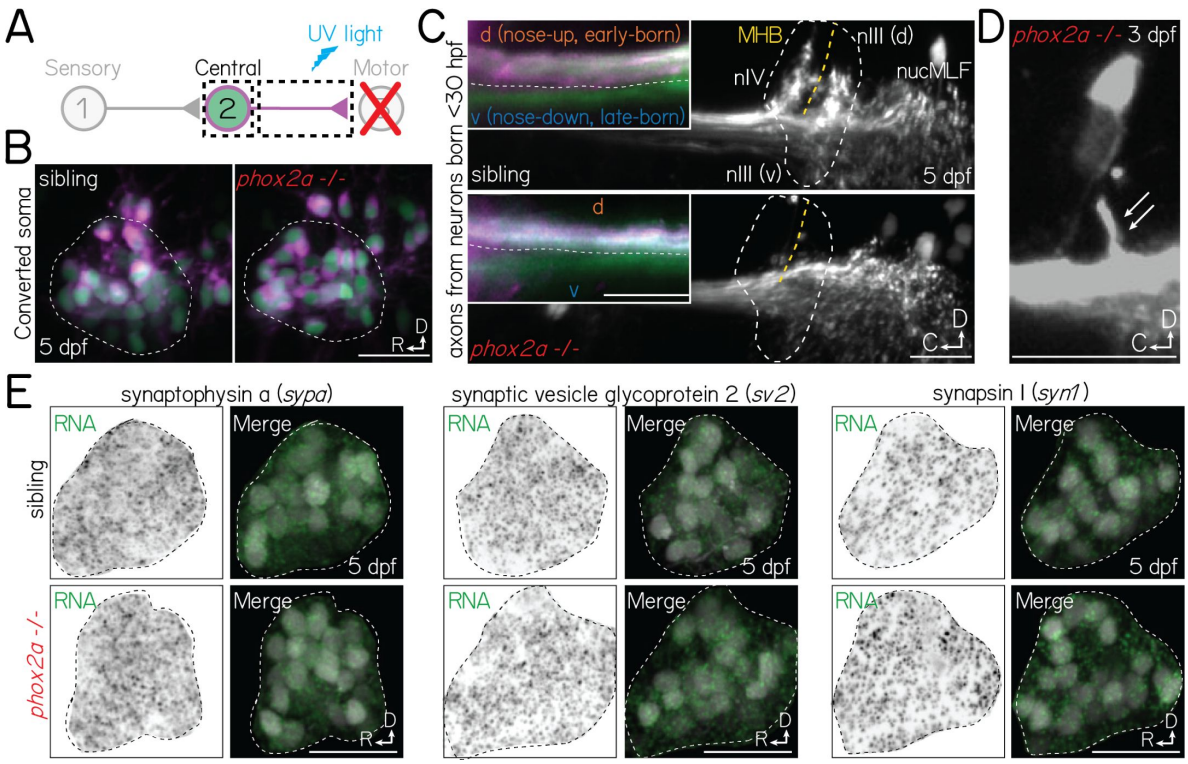

Figure 4

Projection neurons are anatomically and molecularly poised to assemble with motor neuron partners in *phox2a* mutants.

(A) Schematic of retrograde photofill experiments. Projection neuron axons expressing the photolabile protein Kaede are targeted at the midbrain-hindbrain boundary with ultraviolet light. Converted protein (magenta) retrogradely diffuses to the soma, while the unconverted nucleus remains green.
(B) Projection neuron somata in sibling controls (left) and *phox2a* null mutants (right) after retrograde photolabeling. Experiments performed at 5 dpf. Neurons visualized in *Tg(isl1:GFP);Tg(-6.7Tru.Hcrtr2:GAL4-VP16);Tg(UAS:E1b-Kaede)*.
(C) Projection neuron axons at the hindbrain (inset) and midbrain-hindbrain boundary in sibling controls (top) and *phox2a* null mutants (bottom). Axons visualized using *Tg(isl1:GFP);Tg(-6.7Tru.Hcrtr2:GAL4-VP16);Tg(UAS:E1b-Kaede)*. White dashed outline shows arborization fields in nIII/nIV. MHB and yellow dashed line, midbrain-hindbrain boundary. nucMLF: nucleus of the longitudinal fasciculus. Inset: Spatial segregation between early-born (magenta+green) and late-born (green only) axons. White dashed line reflects separation between dorsal (nose-up, early-born) and ventral (nose-down, late-born) axon bundles. Image at 5 dpf in sagittal view.
(D) Projection neuron axon bundle in a *phox2a* null mutant at 3 dpf. White arrows point to single collateral to two remaining nIII/nIV neurons.
(E) Fluorescent *in situ* hybridization against RNA for three pre-synaptic markers: synaptophysin a (*sypa*; left), synaptic vesicle glycoprotein 2 (*sv2*, middle), and synapsin I (*syn1*, right). Top row, sibling controls. Bottom row, *phox2a* null mutants. For each panel set, left images show *in situ* probe expression (green) and right images show merge with projection neurons labeled in *Tg(-6.7Tru.Hcrtr2:GAL4-VP16);Tg(UAS:E1b-Kaede)*. Dashed lines outline the projection nucleus. Cell and transcript expression outside the projection nucleus is removed for visual clarity. Images taken at 5 dpf in sagittal mount. All scale bars, 20 µm.

If motor neurons are required to initiate synaptogenesis, then projection neurons should fail to develop pre-synaptic machinery. To test this hypothesis, we performed fluorescent *in situ* hybridization against common pre-synaptic transcripts: synaptophysin a (*sypa*), synaptic vesicle glycoprotein (*sv2*), and synapsin I (*syn1*). In both *phox2a* mutants and controls, we observed robust transcript expression in projection neuron somata at 5 dpf (**Figure 4E**), well-after synaptogenesis onset in wildtype larvae [29]. Motor partner-derived signals are thus not required for projection neurons to develop the necessary components for synaptogenesis.

Though motor neurons may play later roles in selecting and/or refining pre-motor input specificity, our data supports that projection neurons remain anatomically and molecularly poised to assemble with appropriate targets. We predict that absent collaterals and synapses reflect a lack of adhesive contact necessary to stabilize [45,46], but not instruct the formation of nascent structures.

The transcriptional profiles of projection neurons are intact in the absence of motor partners

Functional and anatomical connectivity, from peripheral sensors to motor targets, develop independently of motor partners. Fate in the vestibulo-ocular reflex circuit follows from connectivity [21], but neuronal fate can also be defined with respect to unique transcriptional signatures. Previously, we developed a sequencing pipeline to discover transcription factors that specify functional subtypes of spinal motor neurons and evaluate the consequences of perturbations on transcriptional fate [47]. We adapted this approach to determine if loss of motor-derived signals changed the transcriptional profiles of projection neurons.

We compared the transcriptional profiles of projection neurons in *phox2a* mutants and sibling controls (**Figure 5A**) using bulk RNA sequencing. We performed sequencing experiments at 72 hours post-fertilization (hpf), after projection neuron differentiation is complete and synaptogenesis to motor targets has peaked [29]. We sequenced projection neurons labeled by *Tg(-6.7Tru.Hcrtr2:GAL4-VP16);Tg(UAS-E1b:Kaede)* [24,25,48,49] (Methods, **Figure 5B**, **Figure S2**). Neurons labeled in this line include, but are not exclusive to the projection neurons in the tangential nucleus used for vertical gaze stabilization. Therefore, we evaluated our bulk RNA sequencing dataset in the context of a single-cell reference atlas derived from the same transgenic line (Methods, **Figure S3**) to minimize noise from other labeled populations. We used *evx2* [50] as a reference, as it was expressed in all projection neurons (**Figure S3D**) and highly detected (50%) in singly-profiled projection neurons.

There were strikingly few differentially-expressed genes in projection neurons between *phox2a* siblings and null mutants (**Figure 5C**, **Table 2**). All candidate differentially-expressed genes were lowly-expressed (detected in <10% of reference projection neurons, **Figure 5D**). To determine if any candidates were differentially expressed in projection neurons, we used a fluorescent *in situ* hybridization method [51] in which fluorescence intensity correlates with detected transcript expression reliably across individual larvae (**Figure S4**). We evaluated 8 candidate genes (**Figure 5E**-**Figure 5F**). Qualitatively, we observed no differences in expression patterns between *phox2a* mutants and siblings, neither in candidates with significant differential expression in the bulk RNA sequencing dataset or in a highly-expressed control markers, *evx2*.

We considered that our inability to detect differentially-expressed genes could arise from our exclusion of candidates based on their expression in our reference single-cell atlas. Therefore, we repeated our analyses in unfiltered bulk sequencing data. The top 50 highest-expressed genes in *phox2a* siblings were highly detected in singly-profiled neurons labeled by *Tg(-6.7Tru.Hcrtr2:GAL4-VP16);Tg(UAS-E1b:Kaede)*, including projection neurons (**Table 3**). This suggests that our dissections adequately captured our target population. However, we again

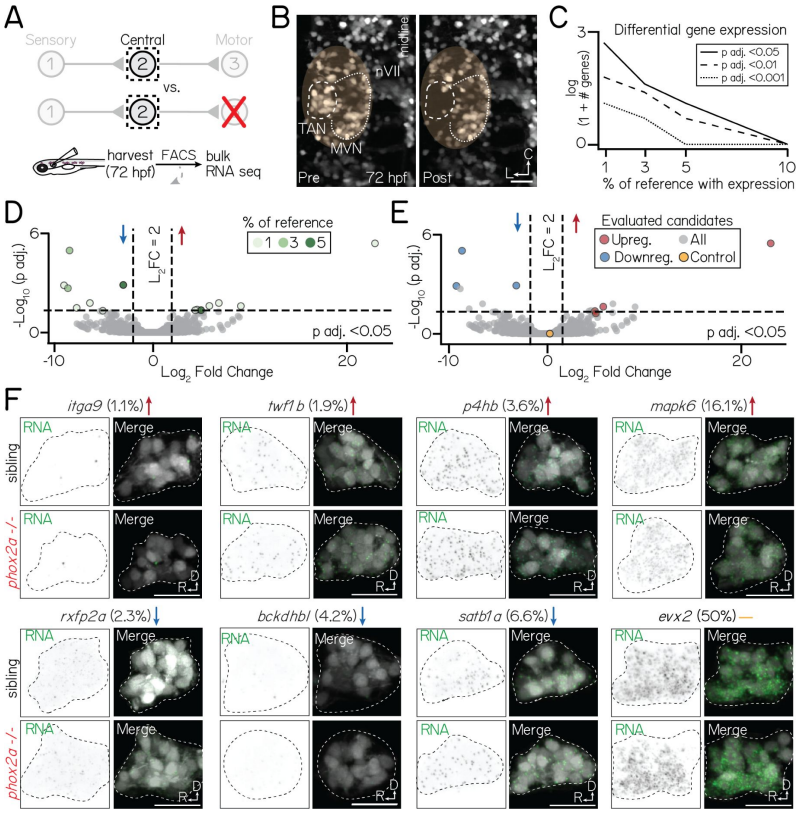

Figure 5

Motor neurons are dispensable for normal transcriptional profiles of projection neurons.

Associated with **Figure S2**-**Figure S5**, **Table 2**.

(A) Schematic of sequencing approach. Central projection neurons (*Tg(-6.7Tru.Hcrtr2:GAL4-VP16)*;*Tg(UAS:E1b-Kaede)*) are harvested from 3 dpf larvae. Flow cytometry is used to exclude neurons not labelled by *Tg(-6.7Tru.Hcrtr2:GAL4-VP16)*. Bulk RNA sequencing is performed to compare the profiles of projection neurons in siblings and *phox2a* null mutants.

(B) Example of projection neurons before (left) and after (right) harvesting. Neurons visualized with *Tg(isl1:GFP)*;*Tg(-6.7Tru.Hcrtr2:GAL4-VP16)*;*Tg(UAS:E1b-Kaede)*. Dashed lines outline projection neurons in the tangential nucleus; dotted lines, medial vestibular nucleus. Yellow region shows margin of harvesting error: non-projection neurons that may be included in bulk sequencing dataset.

(C) Number of differentially expressed genes in projection neurons at 3 dpf after applying progressive filters based on gene expression in a reference single-cell dataset. Data shown on logarithmic scale. Solid, dashed, and dotted lines represent differentially-expressed gene with p adjusted<0.5, p adjusted<0.01, or p adjusted<0.001 significance, respectively.

(D) Volcano plot showing differentially expressed genes in projection neurons between control and *phox2a* null larvae at 3 dpf. Dashed lines represent significance cutoffs: horizontal line, p adjusted>0.05; vertical line, Log_2 Fold Change > 2.0. Each circle is a gene. Genes to the left and right of 0 on the horizontal axis show downregulated and upregulated genes, respectively. Colors indicate percent of reference cells that express a given gene. Grey-colored genes are below both significance thresholds.

(E) Same data as **Figure 5D**. Colored genes show eight candidates evaluated with fluorescent *in situ* hybridization: red, upregulated; blue, downregulated; yellow, highly-expressed controls (*evx2*.

(F) Fluorescent *in situ* hybridization against candidate genes that met projection neuron filter criteria. Top row shows sibling controls; bottom row, *phox2a* null mutants. For each gene, left panels show RNA probe (green) and right panels show merge with projection neurons labeled by *Tg(-6.7Tru.Hcrtr2:GAL4-VP16)* (grey). Dashed lines outline the projection nucleus. Cell and transcript expression outside the projection nucleus is masked for visual clarity. Arrows denote whether genes are upregulated (red), downregulated (blue), or not significantly changed (yellow). Percentage refers to fraction of cells in a single-cell RNA sequencing reference atlas (Methods) with detected transcript. Candidates: *itga9* (log_2 fold change=23.0, p adj.=3.9×10^{-6}), *twf1b* (log_2 fold change=5.9, p adj.=0.024, *p4hb* (log_2 fold change=5.1, p adj.=0.04), *mapk6* (log_2 fold change=5.1, p adj.=0.06), *rxfp2a* (log_2 fold change=-8.5, p adj.=1.1×10^{-5}), *bckdhbl* ((log_2 fold change=-9.1.0, p adj.=0.001) *satb1a* ((log_2 fold change=-3.0, p adj.=0.001), *evx2* (log_2 fold change=0.46, p adj.=0.99). All scale bars, 20 μm.

Gene	% of projection neurons with expression	Putative origin	Log_2 fold change	p adjusted
Upregulated				
** # itga9*	1.1	r4-7	23.0	3.9E-06
# dysf	0.6	r4-7	6.9	0.016
cers3a	3.2	r4-7	9.2	0.024
** # twf1b*	1.9	r4-7, inc. r5-6 inhib	5.9	0.024
# abtb2a	0.4	r4-7, inc. r5-6 inhib	4.7	0.041
** # p4hb*	3.6	r4-7, r5-6 inhib, MNs	5.1	0.044
# fhdc3	1.3	r4-7, r5-6 inhib, MNs	4.5	0.044
Downregulated				
** # rxfp2a*	2.3	r4-7, inc. inhib	-8.5	1.1E-05
** # satb1a*	6.6	r4-7 (inc. inhib), MNs	-3.0	0.001
** # bckdhbl*	4.2	r4-7, glia	-9.1	0.001
# polrmt	4.0	r4-6, inc. MVN	-8.7	0.002
CR847895.1	2.1	r4-6	-6.4	0.016
asns	1.5	r4-7, MNs	-7.8	0.032
BX294160.1	3.6	r4-6	-5.1	0.047

Table 2

Differentially expressed genes in projection neurons.

Star indicates a gene was evaluated using fluorescent *in situ* hybridization. # symbol indicates a gene was also differentially expressed in adjacent medial vestibular neurons (see **Figure S6**). "% of projection neurons with expression" refers to detection in a filtered subset of projection neurons from a single-cell reference atlas of neurons labeled in *Tg(-6.7Tru.Hcrtr2:GAL4-VP16);Tg(UAS-E1b:Kaede)* (Methods, **Figure S3**). Putative origin inferred from gene expression in the annotated 10x dataset (Methods, **Figure S3**)). Genes sorted by p adjusted value. Data associated with **Figure 5**.

identified few differentially-expressed genes in our unfiltered data (**Figure S5A**-**Figure S5C**), with substantial decreases as significance stringency increased. *In situ* hybridization validated that top candidates remained lowly expressed in projection neurons in both *phox2a* siblings and mutants (**Figure S5D**), Importantly, nearly all candidates had low detection across all neurons in our reference single-cell atlas and had predicted expression in populations such as glia and the caudal hindbrain (Methods, **Table 4**). Notably, some candidates were highly expressed in the medial vestibular nucleus, which lies on the medial edge of the tangential nucleus and expressed *phox2a* (**Figure S6**). Together, we conclude that the any differential gene expression in our data either reflects noise or contamination from other labeled populations, but not projection neurons in the tangential nucleus.

We acknowledge the possibility that our *in situ* method is insufficiently quantitative to detect subtle differences in expression. Similarly, despite using both bulk and single-cell RNA sequencing approaches, we may lack the resolution to uncover differential gene expression within projection neurons. Nevertheless, consistent with functional and anatomical characterization, our sequencing data argues that projection neurons acquire the correct transcriptional profiles in the absence of motor partner-derived signals. Our findings are reminiscent of recent reports that the molecular signatures of spinal interneurons develop independently of motor partners [15].

Discussion

Here, we show that motor neurons are dispensable for fate specification in a canonical sensorimotor circuit. We first demonstrated that peripheral sensory and central projection neurons develop appropriate, directionally-selective connectivity and topography independently of their motor partners. Next, we established that projection neurons remain anatomically and molecularly competent to assemble with motor partners. Lastly, we show that loss of motor neurons does not meaningfully alter the transcriptional signatures of their pre-motor projection neuron partners. By providing causal evidence against an instructional role of motor partners for sensory connectivity, our work forces a revision of the current model for vestibulo-ocular reflex circuit formation. As proper connectivity across multiple synapses is foundational for proper function, our work speaks to general mechanisms responsible for sensorimotor circuit assembly.

Transcriptional influences on motor neuron fate specification

While the primary focus of our work was circuit assembly, we found that, unexpectedly, *phox2a* acts in a dose-dependent manner to specify extraocular motor pool fate. Key evidence comes from *phox2a* heterozygotes, in which the earliest-born dorsal neurons in nIII are lost but later-born neurons in nIII/nIV are intact. This observation extends prior characterizations of *phox2a* mutations in zebrafish [34], chick [36], and human [37,38]. Prior work hypothesized that *phox2a* dosage may regulate midbrain motor neuron differentiation into visceral and somatic types [36]. In other systems, transcription [52–54], growth [55] and axon guidance factors [56] can act in such a graded manner to regulate coarse cell type specification and wiring specificity. We extend these ideas to show that *phox2a* dose-dependency acts both over closely-related subtypes (pools within a single cranial nucleus) and along a temporal axis, where partial dosage preferentially targets the earliest-born neurons [33]. Specifically, if *phox2a* is expressed in neural progenitor cells that give rise to nIII/nIV, then the earliest-born motor neurons would have the shortest exposure to *phox2a*.

Molecular insight into ocular motor neuron pool specification is sparse but would be welcome given the strong links between genetic development and ocular motor disease [38,57–59]. For example, subpopulation markers could resolve the topography of pools within dorsal nIII; whether IR/MR pools are spatially segregated or intermingled [33,60]; whether the medial/lateral axis reflects functional differences among motor neuron subtypes; and whether/how local

Gene	% of unfiltered 10x neurons with expression	% of projection neurons
ints5	23.2	33.6
stmn1b	78.6	83.5
sox4a	6.5	13.1
basp1	61.4	56.7
hmgb3a	68.2	67.9
ptmaa	84.5	96.2
gapdhs	28.9	4.2
pnrc2	81.3	89.9
snap25a	65.7	46.9
gpm6ab	81.1	83.9
calm3b	0.0	0.0
marcksl1b	88.8	94.5
tuba1c	59.9	49.0
cd81a	43.3	36.8
meis1b	87.9	95.6
rtn1a	73.4	69.1
elavl3	87.1	93.4
hmgb1b	57.2	65.1
ptmab	80.7	81.2
zc4h2	56.9	64.3
meis2b	57.1	81.6
slc25a5	51.4	37.6
mab21l2	62.7	85.4
h3f3c	69.1	76.5
rtn1b	36.4	22.0
elavl4	78.7	83.5
gng3	37.2	28.3
pik3r3b	77.4	96.0
tubb5	25.3	8.9
histh1l	61.0	74.6
serinc1	51.9	45.0
ckbb	23.5	6.1
oaz1a	43.5	38.9
oaz1b	36.9	27.9
actb1	23.6	2.5
ywhaba	36.2	22.6
ywhag2	36.2	11.6
si:ch211-222l21.1	73.8	87.3
si:dkey-276j7.1	45.8	41.4
aldocb	19.3	2.5
actb2	27.0	5.1
tmem59l	39.8	24.5
calm2b	37.9	19.5
hmgn6	73.6	87.9
h2afx1	59.6	64.7
cd99l2	32.4	20.3
cirbpb	77.8	88.2
ppdpfb	74.5	90.5
stxbp1a	52.3	32.6
Control		
evx2	33.8	50.0

Table 3

Top 50 expressed genes in an unfiltered bulk RNA sequencing dataset of *phox2a* siblings.

"% of unfiltered 10x neurons" refers to gene detection in a single-cell atlas of neurons labeled in *Tg(-6.7Tru.Hcrtr2:GAL4-VP16);Tg(UAS-E1b:Kaede)* (n=1,468 neurons). "% of projection neurons" refers to gene detection in a subset of the single-cell atlas containing projection neurons in the tangential nucleus (n=473 neurons). Data associated with **Figure 5**.

Gene	% of unfiltered 10x neurons with expression	Putative origin	Log_2 fold change	p adjusted
Upregulated				
macc1	0.1	r4-6	24.0	3.2E-06
CR559941.1	0.0		23.7	3.4E-06
si:dkey-65b12.6	0.0		23.5	3.4E-06
si:ch73-106n3.2	0.1		23.5	3.4E-06
mcm10	0.1	MNs	23.4	3.4E-06
si:ch211-244o22.2	0.5	r4-6	23.4	3.4E-06
dre-mir-10a	0.0		23.3	3.5E-06
itga4	0.3	r5-6 (inhibitory)	23.2	3.5E-06
si:dkeyp-87d8.8	0.0		23.2	3.6E-06
arsj	0.5	MNs	23.0	3.9E-06
tlr1	0.0		23.0	3.9E-06
** % itga9*	2.3	r4-7	23.0	3.9E-06
otofb	0.5	r4-6	9.1	1.4E-05
myo7ba	0.4	r4-7	9.8	1.0E-04
zfand1	0.1	MNs	9.0	1.5E-04
% slc22a7a	0.7	r4-7	10.2	1.5E-04
agrp	0.0		13.4	4.1E-04
si:dkey-46i9.6	0.1	r5-7	7.7	6.8E-04
muc2.2	0.0		9.4	6.9E-04
cd37	0.0		9.1	9.8E-04
musk	0.3	r4-6	9.4	1.2E-03
mcamb	0.2	r5-7	8.3	2.7E-03
ppp1r42	0.5	r5-6 (inhibitory)	7.9	3.1E-03
CR677513.1	0.0		9.9	3.5E-03
Downregulated				
** % satb1a*	7.9	r4-7 (inc. inhib), MNs	-8.6	1.0E-06
znf975	0.7	r4-6	-8.3	1.5E-06
phldb1a	0.6	r5-7 (inc. inhib)	-9.2	1.5E-06
TSTA3	0.0		-9.7	3.4E-06
si:dkey-24p1.6	0.0		-8.3	8.4E-06
si:dkey-77f5.14	0.2	r5-7	-8.5	1.1E-05
tha1	0.1	MVN	-10.3	2.1E-05
serpinh2	0.5	r4-6	-9.0	3.7E-05
ghrh	0.3	r4-7	-9.5	6.9E-05
asah1b	0.8	r4-7	-7.8	9.9E-05
msmo1	0.9	r5-7, inc. inhib	-8.9	1.1E-04
tagln2	0.3	glia	-8.4	2.2E-04
zgc:174863	0.1	MNs	-9.9	2.2E-04
** % rxfp2a*	3.2	r4-7, inc. inhib	-6.6	6.8E-04
bmp4	0.7	r4-7	-6.8	6.8E-04
cfl1l	0.1	r4-6	-8.4	6.8E-04
** polrmt*	4.2	r4-7, inc. inhib	-8.8	6.9E-04
anxa2a	0.6	r4-7	-3.0	1.3E-03
galr1a	0.3	MVN	-9.1	1.4E-03
selenow2b	0.1		-8.0	1.8E-03
** % bckdhbl*	1.4	r4-7, glia, MNs	-8.7	2.1E-03
boka	0.5	r5-7	-8.6	2.9E-03
cyldb	0.2	r4-7	-7.9	3.0E-03
pon2	0.6	r4-7, glia, MNs	-5.0	3.1E-03
si:ch73-204p21.2	0.3	r5-7, inc. inhib	-8.2	3.5E-03
and2	0.1	r4-6	-5.8	3.7E-03
Control				
evx2	33.8	r4-7	0.46	0.99

Table 4

Top 50 differentially expressed genes in an unfiltered bulk RNA sequencing dataset of *phox2a* siblings and null mutants.

One star indicates a gene was retained in a filtered subset of projection neurons; %, evaluated using fluorescent *in situ* hybridization. "% of unfiltered 10x neurons" refers to gene detection in an unfiltered single-cell reference atlas of neurons labeled in *Tg(-6.7Tru.Hcrtr2:GAL4-VP16);Tg(UAS-E1b:Kaede)* (n=1,468 neurons). Putative origin inferred from gene expression in the annotated 10x dataset (Methods, **Figure S3**). Genes sorted by p adjusted value. Data associated with **Figure 5**.

interactions between motor neuron pools contributes to fate specification [61]. In spinal circuits, the rich molecular understanding of motor pool specification [47,62–65] has enabled targeted perturbations of pool identity, allowing for major discoveries of their roles in circuit assembly [9,13,15,66]. Our findings thus represent a step forward towards understanding how developmental deficits may contribute to ocular motor disorders [67].

Motor neurons: active or passive architects of pre-motor connectivity?

Our discoveries advance outstanding controversies over whether motor neurons actively or passively shape pre-motor connectivity. We find that extraocular motor neuron axons do not serve as "pioneers" [68–72], with pre-motor axon targeting following passively from motor-derived pathfinding signals [2]. Such a model predicts that projection neuron targeting would be entirely ablated after constitutive loss of extraocular motor neurons and their secreted signals [73–77]. Instead, we observed that projection neurons still establish long-range (hindbrain to midbrain) axonal projections, with appropriate spatial segregation that matches the topography of their motor partners [28,29,33]. Our findings complement reports in spinal circuits that pre-motor targeting is grossly appropriate after manipulating the spatial source of, but not ablating, potential pathfinding signals [13], and that the transcriptional fate of premotor projection neurons similarly develops independently [15]. We point to the late development of ocular musculature [78,79] compared to spinal musculature [2] as a potential source of the dispensability of muscle-derived signals.

Our work is also inconsistent with the strongest form of the "retrograde" hypothesis for vestibulo-ocular reflex circuit assembly. Originally, the retrograde model posited that motor neurons release a diffusable or cell-surface available signal that instructs premotor collaterals to sprout and then innervate specific pools, enabling behavioral specificity [3,31]. Here, the proper spatial and temporal segregation of projection neuron axons suggests they remain poised to wire with spatially-appropriate (dorsal/ventral pools) targets. Additional evidence comes from incomplete *phox2a* knockouts (1-5% of nIII/nIV remaining), where projection neurons still form collaterals, though not robustly or reliably. We predict that projection neuron axons do not require a target-derived cue to grow, search, and synapse onto motor targets, and simply lack the adhesive contact necessary to stabilize nascent structures (reviewed in [45,46]).

Nevertheless, extraocular motor neurons might still play an active or passive role in selecting and/or refining input specificity from their projection neuron partners. In spinal circuits, motor pool position passively imposes geometric constrains on pre-motor axon targeting [13,14], and manipulating the dendritic structure of motor neuron axons transforms input specificity [9,11]. Genetic perturbations of nIII/nIV motor neuron position selectively compromise ocular responses to directional visual stimuli [61], though the circuit-level origin of such impairments is unclear. For the vestibulo-ocular reflex circuit, transforming all motor pools to the same fate or genetically "scrambling" pool position could resolve whether motor input specificity is truly hard-wired in projection neurons, or whether projection neurons instead target gross spatial domains irrespective of partner identity [13]. Motor neuron-derived signals are of course capable of shaping their input by strengthening/weakening their inputs. Importantly, our results suggest that such signals will not define the fate of projection neurons, and by extension, circuit architecture.

We note that our study does not eliminate one additional source of post-synaptic partner signals to projection neurons. As in primates [80], projection neurons also contact neurons in the interstitial nucleus of Cajal, also known as the nucleus of the medial longitudinal fasciculus (INC/nMLF) [24]. INC/nMLF neurons project early in development [81] to spinal circuits used for postural stabilization during swimming [82–86]. Notably, ablation of projection neurons disrupts postural stability [50]. As we did not observe postural deficits in *phox2a* mutants, we infer that projection neuron connectivity to INC/nMLF targets is present and functional. Correspondingly, the

development of projection neuron collaterals and synapses to INC/nMLF neurons appeared qualitatively normal in *phox2a* mutants, supporting our interpretation that projection neurons retain the capacity to properly assemble with post-synaptic targets even though similar structures to extraocular motor neurons are absent. In the future, if a similarly specific marker like *phox2a* is identified that labels the INC/nMLF, it will be possible to test whether these neurons play a role in vestibulo-ocular reflex circuit development.

Alternative mechanisms for fate specification and sensory input specificity in projection neurons

What is the origin of signals that govern projection neuron fate and sensory input specificity, if not motor-derived? In comparable systems, fate signals can be intrinsically-expressed or originate from extrinsic sources. For example, intrinsic genetic mechanisms assemble laminar connectivity in visual circuits [87,88] and facilitate sensorimotor matching in spinal circuits [9,89–91]. In directionally-selective retinal circuits, subtype fate is established in a similar manner [92,93]. In "intrinsic" models, synaptic specificity arises from molecular matching between subtypes [94–96]. Alternatively, in somatosensory and auditory circuits, transcriptional fate depends on extrinsic signals such as growth factors [97] and sensation [98], respectively. In spinal circuits, positional fate, which constrains connectivity [13], is established by extrinsic codes such as morphogen gradients in early development [99] and Hox factors [63,64]. In "extrinsic" models, early inputs are often erroneous and refined by activity [100,101] or molecular factors [102]. Collectively, these findings offer two alternative models for how vestibulo-ocular reflex circuit assembly emerges.

The tight links between birth order, somatic position, and stimulus selectivity [28,29,33,85,103,104] across vestibulo-ocular reflex circuit populations support an "intrinsic" determination model. Further, neurogenesis and initial axon targeting develops contemporaneously for sensory afferents [55,103,105,106], projection neurons [3,29,107–109], and extraocular motor neurons [3,33,39,110–112], suggesting that neurons are poised to assemble with targets as early as their time of differentiation. Importantly, an "intrinsic specification" model makes a testable prediction about how and when sensory selectivity should emerge across the circuit: projection neurons and extraocular motor neurons should be directionally selective as soon as pre-synaptic input is established. Such evidence would justify future molecular inquiries into the underlying genetic factors, expanding early characterizations of the mechanisms that shape hindbrain topography [113,114], recent molecular profiling of the zebrafish hindbrain [115,116], and reports of molecular matching between extraocular motor neurons and muscle [117,118]. Operationally, the present study lays a foundation for molecular explorations of projection neuron subtype determinants by establishing bulk- and single-cell transcriptomic profiling and *in situ* validation pipelines.

Conversely, evidence that stimulus selectivity emerges gradually would suggest that sensory afferents and/or projection neurons initially wire indiscriminately and that circuit connectivity is refined in time by extrinsic forces. Prior work in the vestibuloocular reflex circuit has proposed developmental roles for sensory-derived trophic factors [119] and activity-dependent refinement [120,121], though sensory afferents develop typically in the absence of utricular input [122] and ocular motor behavior does not depend on stimulus-driven activity [123]. Here, an "extrinsic" determination model would predict that connectivity is established by an anterogradely-transmitted signal – that is, from sensory afferents to ocular muscles. If so, then future investigations might constitutively ablate sensory afferents to eliminate activity-driven, diffusible, or cell-surface instructional signals, similar to the present study. The directional bias in opsin-evoked activity in projection neurons [25], together with their transcriptional profiles established here, offer a clear readout of the role of sensory-derived factors. However, genetic targets exclusive to vestibular sensory afferents for gaze stabilization have not been identified, and tissue-specific genetic ablations remain limited in zebrafish. Looking ahead, resolving when and how

stimulus selectivity emerges across the vestibulo-ocular reflex circuit will be key to understanding whether connectivity with pre- and/or post-synaptic partners instructs subtype fate, or whether subtype fate instructs connectivity.

Conclusion

Here, we discovered that motor partners do not determine pre-motor fate and sensory connectivity for the projection neurons that stabilize gaze. Our results overturn the current model that stimulus selectivity and connectivity are retrogradely specified, a major step towards understanding the origin, and eventually nature, of mechanisms that assemble an archetypal sensorimotor reflex circuit. Instead, our data support and extend recent models in spinal systems that motor partners do not actively construct sensory- to-interneuron reflex circuit architecture, but may later refine their inputs. By defining the contribution of motor neurons to specification and sensory connectivity of gaze-stabilizing central projection neurons, our work speaks to general principles of sensorimotor circuit assembly.

Materials and methods

Resource availability

Lead Contact

Further information and requests for resources and reagents should be directed to and will be fulfilled by the lead contact, David Schoppik (schoppik@gmail.com).

Materials Availability

Mutant fish lines generated in this study will be deposited to the Zebrafish International Resource Center (ZIRC).

Data and code availability

- All data and code are deposited at the Open Science Framework and are publicly available at DOI: 10.17605/OSF.IO/93V6E

Experimental model and subject details

Fish care

All protocols and procedures involving zebrafish were approved by the New York University Langone School of Medicine Institutional Animal Care & Use Committee (IACUC). All larvae were raised at 28.5°C at a density of 20-50 larvae in 25-40 ml of buffered E3 (1mM HEPES added). Larvae used for photofill experiments were raised in constant darkness; all other fish were raised on a standard 14/10h light/dark cycle. Larvae for experiments were between 3-5 days post-fertilization (dpf).

Transgenic lines

Experiments were conducted on the *mifta*$^{-/-}$ background to remove pigment. All experiments used larvae from the F3 generation or older of a newly-created line of *phox2a* mutants (described below) on the following backgrounds: *Tg(isl1:GFP)* [40] to validate *phox2a* loss-of-function; *Tg(isl1:GFP);Tg(-6.7Tru.Hcrtr2:GAL4-VP16)* [25,49] to drive UAS reporter expression; *Tg(UAS-E1b:Kaede)* [48] for anatomical imaging experiments; and *Tg(UAS:GCaMP6s)* [83] for calcium imaging experiments. All larvae were selected for brightness of fluorescence relative to siblings. Mendelian ratios were observed, supporting that selected larvae were homozygous for fluorescent reporter alleles.

Generation of *phox2a* mutants

phox2a mutant lines were generated using CRISPR/Cas9 mutagenesis. Two guide RNAs (gRNAs) were designed using the Benchling CRISPR Guide RNA Design Tool (see: key resources, **Table 5**). gRNAs were located towards the 5' region of exon 1 to minimize the size of any translated protein. gRNAs were incubated with Cas9 protein before co-injection into *Tg(isl1:GFP)* embryos at the single cell stage. Injected embryos were screened for anatomical phenotypes (reduction in *isl1*-positive nIII/nIV motor neurons). Phenotypic embryos (F0) and their embryos were raised and genotyped via sequencing to identify and validate germline mutations. Three founders were identified and used for experiments: (1) *phox2a*^{d22} has a 22 bp deletion from base pairs 249 to 270, (2) *phox2a*^{d19} has a 19 bp deletion from base pairs 262 to 280, and (3) *phox2a*^{i2} has a 2 bp insertion (AG) from base pairs 261 to 262. Each mutation created a nonsense mutation, causing a predicted premature stop codon at the beginning of the homeobox. All alleles were validated using complementation assays, and larvae from all three alleles were used in experiments. For brevity, only one allele (*phox2a*^{d22}) is shown in **Figure 1**.

Maintenance of *phox2a* adults

phox2a null larvae do not survive past 7 dpf. Sibling embryos (*phox2a*$^{+/+}$ or *phox2a*$^{+/-}$) were raised and genotyped to identify heterozygotes for line propagation. Primers for genotyping are listed in the Key Resources table (**Table 5**). Genomic DNA was amplified using a polymerase (DreamTaq PCR Master Mix 2X, Thermo Fisher Scientific K1071), 60°annealing temperature, 30 second elongation time, and 35 cycles of PCR. PCR generates a 169 bp product (wildtype), 147 bp product (*phox2a*^{d22}), 150 bp product (*phox2a*^{d19}), or 171 bp product (*phox2a*^{i2}). *phox2a*^{d22} and *phox2a*^{d19} DNA was evaluated using gel electrophoresis; *phox2a*^{i2} was assessed via sequencing with the reverse primer (Genewiz, Azenta Life Sciences, South Plainfield, New Jersey).

Method details

Confocal imaging

Larvae were anesthetized in 0.2 mg/mL ethyl-3-aminobenzoic acid ethyl ester (MESAB, Sigma-Aldrich E10521, St. Louis, MO) prior to confocal imaging except where noted. Larvae were mounted dorsal side-up (axial view) or lateral side-up (sagittal view) in 2% low-melting point agarose (Thermo Fisher Scientific 16520) in E3. Images were collected on a Zeiss LSM800 confocal microscope with a 20x water-immersion objective (Zeiss W Plan-Apochromat 20x/1.0). Images of tangential nucleus soma and axons were acquired in a lateral mount with an 80×80 µm imaging window. Stacks spanned ~30-40 µm, sampled every 1 µm. Images of nIII/nIV motor neurons were acquired in a dorsal mount with a 213×106 µm imaging window; stacks spanned approximately 90 µm, sampled every 1.5 µm. Images to validate nIII/nIV expression in a lateral mount were acquired using a 319×319 µm imaging window. Raw image stacks were analyzed using Fiji/ImageJ [124].

REAGENT or RESOURCE	SOURCE	IDENTIFIER
Chemicals, peptides, and recombinant proteins		
Tween	Fisher Scientific	BP337-100
32% paraformaldehyde	Electron Microscopy Sciences	15714
Proteinase K	ThermoFisher Scientific	25530049
Papain	Worthington Biochemical	LK003178
Hanks Buffered Salt Solution (HBSS)	ThermoFisher Scientific	14170112
Earl's Buffered Salt Solution (EBSS)	ThermoFisher Scientific	24010043
DNAse	Worthington Biochemical	LK003172
DAPI	Invitrogen	D1306
L15 Medium	ThermoFisher Scientific	11415064
Fetal bovine serum, qualified, triple-filtered	ThermoFisher Scientific	A3160501
Collagenase Type 1A	Sigma Aldrich	C9891-500MG
Low melting point agarose	ThermoFisher Scientific	16520
Ethyl-3-aminobenzoic acid ethyl ester (MESAB)	Sigma Aldrich	E10521
Pancuronium bromide	Sigma Aldrich	P1918
Critical commercial assays		
in situ hybridization chain reaction v3.0 (HCR)	Molecular Instruments	N/A
RNAqueous Micro Total RNA Isolation Kit	ThermoFisher Scientific	AM1931
MEGAshortscript T7 Transcription Kit	ThermoFisher Scientific	AM1354
QiaQUICK PCR Purification Kit	Qiagen	28104
EnGen Spy Cas9 NLS	New England Biolabs	M0646T
Deposited data		
Raw and analyzed calcium imaging data	This study	DOI: 10.17605/OSF.IO/93V6E
Raw and analyzed 10x Genomics scRNA-seq datasets	This study	GEO: accession number forthcoming
Raw and analyzed bulk RNA seq datasets	This study	GEO: accession number forthcoming
Experimental models: Organisms/strains		
Tg(-6.7Tru.Hcrtr2:GAL4-VP16)	[25,49]	ZFIN: ZDB-TGCONSTRCT-151028-8
Tg(UAS-E1b:Kaede)	[48]	ZFIN: ZDB-TGCONSTRCT-070314-1
Tg(isl1:GFP)	[40]	ZFIN: ZDB-ALT-030919-2
Tg(UAS:GCaMP6s)	[42]	ZFIN: ZDB-TGCONSTRCT-140811-3
phox2a^{d22}	This study	N/A
phox2a^{d19}	This study	N/A
phox2a^{i2}	This study	N/A
Oligonucleotides		
phox2a forward primer (5-CAGCCAGAGCAACGGCTTCC-3)	Sigma Aldrich	N/A
phox2a reverse primer (5-AAGCCGACAACAGTGTGTGTGTAA-3)	Sigma Aldrich	N/A
phox2a guide 1 (5-CTCGCCACCGCCAGCTGCAC-3)	Sigma Aldrich	N/A
phox2a guide 2 (5-CTCCGGCTTCAGCTCCGGCC-3)	Sigma Aldrich	N/A
HCR probes	Integrated DNA Technologies	N/A
Software and algorithms		
Fiji/ImageJ	[124]	RRID: SCR_02285
Adobe Illustrator (2021)	Adobe	RRID: SCR_010279
Matlab 2020b	Mathworks	RRID: SCR_001622
Seurat v4	[133]	https://satijalab.org/seurat
CRISPR Guide RNA Design Tool	Benchling	https://benchling.com/crispr
Other		
20 micron cell strainer	pluriSelect	431002060
SH800z 100 micron sorting chip	Sony	LE-C3210

Table 5

Key Resources Table (associated with Methods).

Identification of *phox2a* larvae

Prior to experiments, larvae were designated as *phox2a* mutants or sibling (wildtype/heterozygote) controls based on two criteria: gross loss of *Tg(isl1:GFP)* fluorescence in nIII/nIV at 2 dpf, visualized using a SugarCube LED Illuminator (Ushio America, Cypress CA) on a stereomicroscope (Leica Microsystems, Wetzlar, Germany) and absence of a swim bladder at 5 dpf. For anatomical and calcium imaging experiments, allele designations were validated using confocal imaging of nIII/nIV motor neurons: total or near-total loss of nIII/nIV neurons (null), selective loss of IR/MR neurons (heterozygote), or normal expression (wildtype). Designations were confirmed after experiments using genotyping. For RNA sequencing and fluorescent *in situ* experiments, sibling controls (wild-type/heterozygote) were combined.

Birthdating of nIII/nIV motor neurons

Early-born neurons in nIII/nIV were optically tagged using *in vivo* birthdating [29,33,125] on *Tg(isl1:Kaede)*^{ch103} larvae [126]. Briefly, whole embryos were exposed to UV light for five minutes at experimenter-defined timepoints and subsequently raised in darkness to prevent background conversion. At 5 dpf, larvae were imaged on a confocal microscope. Neurons born before the time of photo-conversion expressed red, converted Kaede; neurons born after expressed only green, unconverted Kaede.

Fluorescent *in situ* hybridization and imaging

Experiments were performed using Hybridization Chain Reaction (HCR) for whole-mount zebrafish larvae [51,127]. Probes were generated using the HCR 3.0 probe maker [128] using the sense sequence of the canonical gene cDNA from NCBI. All larvae were from the *Tg(isl1:GFP);Tg(-6.7Tru.Hcrtr2:GAL4-VP16);Tg(UAS-E1b:Kaede)* background. Larvae were pre-identified as null mutants or siblings (wildtype or heterozygotes) and combined in equal ratios (8-10 larvae per condition, 16-20 larvae total) into a single 5 mL centrifuge tube for fixation and HCR. Larvae were fixed overnight with 4% PFA in PBS at 4° C and stored in 100% methanol at - 20° C. Subsequently, HCR was performed as described in [127], with adjustments to proteinase K incubation time based on age (3 dpf: 30 min incubation; 5 dpf: 50 min incubation). HCR experiments used buffers and amplifiers from Molecular Instruments (Los Angeles, CA). Samples were stored in 1x PBS at 4° C and imaged on a confocal microscope within four days. Prior to imaging, larvae were re-screened for *Tg(isl1:GFP)* fluorescence to identify null mutants and sibling controls. For each probe, imaging parameters were determined using a sibling control and kept constant for all subsequent larvae. Comparable settings (within 1% laser power) were used across probes.

Calcium imaging of tonic and impulse tilt stimuli responses

Experiments were performed as described in [29] using Tilt-In-Place Microscopy [41]. All experiments used 5 dpf larvae from the *Tg(isl1:GFP);(Tg(-6.7Tru.Hcrtr2:GAL4-VP16);Tg(UAS:GCaMP6s)* background. Briefly, larvae were mounted dorsal-up in 2% low-melt agarose in E3 onto a large beam diameter galvanometer system (ThorLabs GVS011). Tonic pitch-tilt stimuli were presented over a 65-second period in the following order: horizontal baseline (5 sec at 0°), nose-down tilt (15 sec at −19°), horizontal imaging (15 sec at 0°), nose-up tilt (15 sec at 19°), and horizontal imaging (15 sec at 0°). Impulse stimuli contained a 4 msec eccentric rotation, a 2 msec hold, and a 4 msec restoration step to horizontal and were presented twice over a 65-second imaging window: horizontal baseline (20 sec), impulse (10 msec), horizontal imaging (30 sec), impulse (10 msec), horizontal imaging (15 sec). Tonic and impulse stimuli were presented in alternating sets (impulse, then tonic) with a total of three stimulus set repeats.

Imaging was performed using a 20x water immersion objective (Olympus XLUMPLFLN20xW 20x/1.0), an infrared laser (Spectra-Physics MaiTai HP) at 920nm using 6.1-18.8 mW of power at the sample, and ThorLabs LS 3.0 software. Experiments were conducted in the dark. High-resolution anatomy scans of nIII/nIV motor neurons were performed for each experiment to validate allele designations. Scans used a 147×147 µm imaging window, a 90 µm stack sampled every 1.5 µm, and a 5.2 microsecond pixel dwell time. Anatomy scans of the tangential nucleus were acquired using a 148×x91 µm imaging window as a 40-50 µm stack sampled every 1 µm. For stimulus imaging, the tangential nucleus was sampled every 3-6 µm based on cell density. 6-10 planes were sampled for each hemisphere. Ventral planes were imaged at higher magnification (112×68 µm imaging window) than dorsal planes (148×91 µm window) to avoid photomultiplier tube saturation from in-frame GFP fluorescence; magnification was corrected for in later analyses. Laser power was adjusted for each sampled plane due to the light scattering properties of zebrafish tissue. As greater power was required for ventral planes, imaging was always performed from ventral to dorsal to minimize photobleaching effects. Stimulus imaging was performed at 3 frames/second (2.2 µs pixel dwell time) with a total time of approximately two hours per fish.

Retrograde photolabeling of tangential nucleus neurons

Experiments were performed as described in [29] based on [44] on 5 dpf larvae from the *Tg(isl1:GFP)*;*Tg(-6.7Tru.Hcrtr2:GAL4-VP16)*;*Tg(UAS-E1b:Kaede)* background. Briefly, experiments leveraged a photoconvertible protein, Kaede, which irreversibly converts from green to red with ultraviolet light. Larvae were raised in darkness to minimize background conversions. Larvae were mounted dorsal-up in 2% agarose under a confocal microscope. An imaging window was centered over the medial longitudinal fasciculus (MLF) and repeatedly scanned with a 405 nm laser for 30 seconds until fully converted (green to red). Off-target photo-conversion was assessed (e.g., conversion of projections lateral to the MLF). Larvae were unmounted, left to recover in E3 for 4 hours in darkness, and then re-mounted in a lateral mount. An imaging window was centered around the tangential nucleus (see: Confocal Imaging). Retrogradely-labeled soma were identified by their center-surround fluorescence appearance: red converted cytoplasm surrounding an unconverted green nucleus.

Neuron harvesting, dissociation, and flow cytometry

Experiments were performed on 72-74 hpf larvae from the *Tg(isl1:GFP)*;*Tg(-6.7Tru.Hcrtr2:GAL4-VP16)*;*Tg(UAS-E1b:Kaede)* back-ground. At 2 dpf, larvae were designated as null or sibling (wildtype/heterozygote) as described above. Three experimenters (D.G., K.R.H., and P.L) harvested neurons in parallel. Larvae were anesthetized in MESAB in Earle's Balanced Salt Solution with calcium, magnesium, and phenol red (EBSS, Thermo Fisher Scientific 24010043) and mounted dorsal-up in 2% agarose. Fluorescence in tangential nucleus neurons was visualized using a SugarCube LED Illuminator (Ushio America, Cypress CA) using 10x eyepieces on a stereomicroscope (Leica Microsystems, Wetzlar, Germany). Neurons were harvested using a thin wall glass capillary tube (4 inch, OD 1.0 MM, World Precision Instruments) into EBSS in a non-stick Eppendorf tube and kept on ice until dissociation.

Neurons were dissociated in 20 units/mL of papain prepared in EBSS (Worthington Biochemical), 2000 units/mL of deoxyribonucleic prepared in EBSS (Worthington Biochemical), and 100 mg/mL of Type 1A Collagenase (Sigma Aldrich) prepared in Hanks Buffered Salt Solution without calcium/magnesium (HBSS, Thermo Fisher Scientific). Neurons were incubated for 45 minutes at 31.5°C with a gentle vortex every 10-15 min, then passed through a 20 µm filter and centrifuged for 10 mins at 300 x g. After removing supernatant, neurons were resuspended in L15 (Thermo Fisher Scientific) with 2% fetal bovine serum (Thermo Fisher Scientific). Cell health was evaluated using DAPI, applied at 0.5 µg/ml (Invitrogen) and incubated on ice for 30-45 mins prior to flow cytometry.

Flow cytometry was performed using a Sony SH800z cell sorter (100 µm nozzle, 20 psi) to isolate single neurons (**Figure S2**). Three controls were run: (1) non-fluorescent wildtype neurons, (2) non-fluorescent neurons + DAPI, (3) fluorescent (green) neurons from *Tg(isl1:GFP)*;*Tg(-6.7Tru.Hcrtr2:GAL4-VP16)*;*Tg(UAS-E1b:Kaede)* + DAPI. On average, 2% of neurons were DAPI-positive and excluded. Neurons were evaluated for positive (green) fluorescence. Fluorescence was not evaluated to separate *Tg(UAS-E1b:Kaede)* neurons from those labeled by *Tg(isl1:GFP)*. Neurons were sorted into an Eppendorf tube containing 700 µl of lysis buffer (RNAqueous Micro Total RNA Isolation Kit, Thermo Fisher Scientific) for downstream bulk RNA sequencing.

Bulk RNA sequencing

RNA isolation was performed using an RNAqueous Micro Total RNA Isolation Kit (Thermo Fisher Scientific). RNA concentration and quality (RIN > 8.0) was evaluated using an RNA 6000 Pico Kit and a 2100 Bioanalyzer system (Agilent Technologies, Santa Clara, California). RNA sequencing was performed by the NYU Genome Technology Center. Libraries were prepared using the low-input Clontech SMART-Seq HT with Nxt HT kit (Takara Bio USA) and sequenced using an Illumina NovaSeq 6000 with an S1 100 Cycle Flow Cell (v1.5).

Quantification and statistical analysis

Cell counting and spatial mapping of nIII/nIV motor neurons

Analysis was performed in Fiji/ImageJ [124] using the Cell Counter plugin. Anatomical stacks of nIII/nIV were subdivided in the dorsoventral axis as described in [33] to facilitate localization. A point ROI was dropped over each neuron in the plane in which the soma was brightest (center). The number of neurons in each dorsoventral plane and their coordinates were recorded. Neuron coordinates were standardized relative to a (0,0) point, defined as one corner of a standard-sized rectangular box centered over the extent of nIII/nIV in a maximum intensity projection. Differences in spatial location across genotypes was evaluated separately for each spatial axis using a two-tailed, two-sample Kolmogorov-Smirnov test. Probability distributions for figures were generated using the mean and standard deviation from bootstrapped data (n=100 iterations) to ensure results were robust to data from single larva.

Analysis of calcium imaging experiments

Analysis methods are detailed in [29] and summarized briefly here. Regions of Interest (ROIs) were drawn around tangential nucleus neurons for each stimulus plane sampled and adjusted for minor movement (1-2 µm) between trials. Raw fluorescence traces were extracted using Matlab R2020b (MathWorks, Natick, Massachusetts) and normalized by ROI size to account for variation in magnification. A neuron's response to tonic or impulse stimuli was defined as the change in fluorescence in the first second of restoration to horizontal following tilt delivery. Responses were normalized using a baseline period, defined as the mean fluorescence across the initial baseline window (5 sec) preceding the nose-down tilt (nose-down response) or the last 3 sec of the horizontal restoration following nose-down tilt (nose-up response). This was used to generate a ΔFF value. A ΔFF response was defined as significant if it was greater than two standard deviations above baseline. Directional selectivity was assigned by normalizing the difference in ΔFF responses to each tilt by their sum. This generated a scale of values of ±1 (i.e., positive values represent nose-up selectivity; negative values, nose-down). Some neurons responded to both tilt directions with high similarity; we set a minimum threshold of abs(0.1) to distinguish neurons with a clear directional selectivity from untuned neurons.

Spatial mapping of tangential nucleus neurons

Analysis methods are detailed in [29] and summarized briefly here. All imaged neurons were manually registered to a reference framework using Adobe Illustrator (2021). Anatomy stacks from all experiments were aligned in the XY (rostrocaudal, mediolateral) axes using established anatomical landmarks (e.g., Mauthner cell body, medial longitudinal fasciculus, otic capsule). For Z-registration (dorsoventral axis), stacks were subdivided into eight sections using landmarks within and around the tangential nucleus (e.g., Mauthner cell body, neuropil). All registered images were verified by two independent observers (D.G. and S.H.). Neurons were localized to one dorsoventral section and a reference circle, representing a cell, was placed in Illustrator. Coordinates for each reference circle were recorded and standardized to an absolute (0,0) point (dorsomedial-most point of the tangential nucleus). Coordinates were imported into Matlab (R2020b) and used to generate a spatial map of imaged neurons.

Statistical analysis of differences in tilt responses across *phox2a* genotypes

Statistical comparisons of tonic and impulse tilt responses are summarized in **Table 1**. Analyses used a one-way analysis of variance with multiple comparisons. No significant differences (tonic tilt responses) or small differences (impulse responses) were observed across genotypes. Control data reported in Results and **Figure 2**-**Figure 3** is an aggregate from wildtype, *phox2a*$^{+/+}$, and *phox2a*$^{+/-}$ larvae.

Alignment, quality control, and differential expression analysis of bulk sequencing data

Initial alignment and analyses were performed by the Applied Bioinformatics Laboratories at the NYU School of Medicine (RRID:SCR_019178). Sequencing data was aligned to the GRCz11 zebrafish reference genome and two fluorescent markers (Kaede, GFP; NCBI). Eight datasets from four experimental repeats were aligned: four from *phox2a* mutants, and four from sibling controls. One experimental repeat had significantly higher variance in the first and second principal components, likely due to poor quality leading to extremely low transcript counts, and was excluded from downstream analyses. Number of cells/larvae sequenced and used in downstream analysis are as follows: Repeat 1, n=532/n=904 cells from N=28/N=28 *phox2a* null/control larvae; Repeat 2, n=802/n=683 cells from N=27/N=26 *phox2a* null/control larvae; Repeat 3, n=1000/n=1007 cells from N=41/N=40 *phox2a* null/control larvae; Repeat 4 (excluded): n=690/n=571 cells from N=33/N=33 *phox2a* null/control larvae Differential gene expression between conditions (*phox2a* mutants vs. sibling controls) was assessed using DESeq2[129]. Differentially-expressed candidate genes met two criteria: $\log_2$ fold change $>|2|$ and p adjusted < 0.05.

Filtering of bulk sequencing data using a reference single-cell sequencing dataset

Analyses were performed in R. Detection of markers for motor neurons (*isl1, isl2a, isl2b*) [130,131] and neurons caudal (*hoxd4a*) [113,132] and lateral (*barhl2*) [114] to rhombomeres 4-6 supported that our dataset included other populations. We applied a filter to exclude erroneous gene expression from non-tangential nucleus populations.

Filtering was performed using an existing single-cell atlas of neurons labeled in *Tg(-6.7Tru.Hcrtr2:GAL4-VP16);(Tg(UAS-E1b:Kaede)*, generated with 10x Genomics. The reference atlas was generated from four experimental samples using the harvest, dissociation, and flow cytometry method described above. The sequenced atlas contained 1,468 neurons (**Figure S3A**-**Figure S3B**)). Data was analyzed using Seurat v4.0 [133]. Cluster annotation was performed

using a combination of fluorescent *in situ* hybridization as described above (**Figure S3C**-**Figure S3E** and other data not shown) and published molecular data of the zebrafish hindbrain [113]. n=473 neurons (32%) were validated as excitatory projection neurons from the tangential nucleus.

Genes in the bulk dataset were only included in downstream analyses if they were expressed above threshold percent of reference projection neurons: 1%, 3%, 5%, 10%, 30%, or 50%. The most stringent filter (50%) was set using the transcription factor *evx2*, which is reported to be expressed in all tangential nucleus neurons [50] and was detected in 50% of reference projection neurons. Qualitatively, we found that gene detection with fluorescent *in situ* hybridization scaled with reference filter stringency (**Figure S4**). Analyses were performed separately for each threshold. The total number of genes included for downstream analyses for each threshold are as follows: 28,807 (no threshold), 11,189 (1% of reference neurons), 7,871 (3%), 6,075 (5%), 3,579 (10%), 818 (30%), 288 (50%). We used the following significance thresholds for differential gene expression in filtered datasets: adjusted p value < 0.05 and abs(log2FoldChange) > 2. The number of differentially expressed genes for each threshold was as follows: 91 (no threshold), 14 (1% of reference neurons), 3 (3%), 2 (5%), 0 (10%).

Projection neurons in the tangential nucleus are transcriptionally similar to excitatory neurons in the medial vestibular nucleus (MVN; unpublished data). MVN neurons may be included in our bulk sequencing dataset given their exceptionally close proximity (3-5 μm) to the medial edge of the tangential nucleus. Some MVN neurons express *phox2a* (**Figure S6**). To control for the possibility that some differentially expressed genes are localized to the MVN, and not projection neurons, we also evaluated differential gene expression in a validated subset of excitatory MVN neurons (n=271 neurons; 18% of reference dataset) from the same single-cell atlas. Data is shown in **Figure S6**.

Generation of representative images for fluorescent *in situ* hybridization

Images were generated using Fiji/ImageJ [124]. An anatomical template of the tangential nucleus was generated based on [29]. Briefly, for sagittal view images, a 30-μm stack was centered over the tangential nucleus. For each plane, a region of interest (ROI) was drawn over all cells within the bounds of the tangential nucleus. Transcript expression outside the ROI was masked. Maximum intensity projections were generated. Minimal or no alterations to brightness/contrast were made for probe expression given the correlation between fluorescence intensity and detected transcript [51].

Additional statistics

Bias and variability in probability distributions were estimated by bootstrapping, or resampling the raw distributions with replacement [134]. Data shown is the mean and standard deviation of 100 bootstrapped distributions. Topography data was evaluated using two-tailed, two-way Kolmogorov-Smirnov tests. Functional responses to tilts (i.e., calcium response strength, directionality index) were evaluated using two-tailed Wilcoxon rank sum tests. Differences in responses across genotypes were analyzed using one-way analysis of variance tests.

Acknowledgements

Research was supported by the National Institute on Deafness and Communication Disorders of the National Institutes of Health under award numbers R01DC017489, F31DC020910, and F31DC019554, the National Institute of Neurological Disorders and Stroke under award numbers F99NS129179, T32NS086750, and the National Cancer Institute P30CA016087. The authors would like to thank Hannah Gelnaw for assistance with fish care, and Jeremy Dasen, Claude Desplan,

Katherine Nagel, Dan Sanes, along with the members of the Schoppik and Nagel labs for their valuable feedback and discussions. Finally, the authors gratefully acknowledge the late Hans Straka for his generous insights and encouragement throughout.

Author contributions

Conceptualization: DG and DS, Methodology: DG, BR, KRH, PL, and DS, Investigation: DG, BR, KRH, PL, ML, HP, HG, SH, and CQ, Visualization: DG, Writing: DG, Editing: DS, Funding Acquisition: DG and DS, Supervision: DS.

Author competing interests

The authors declare no competing interests.

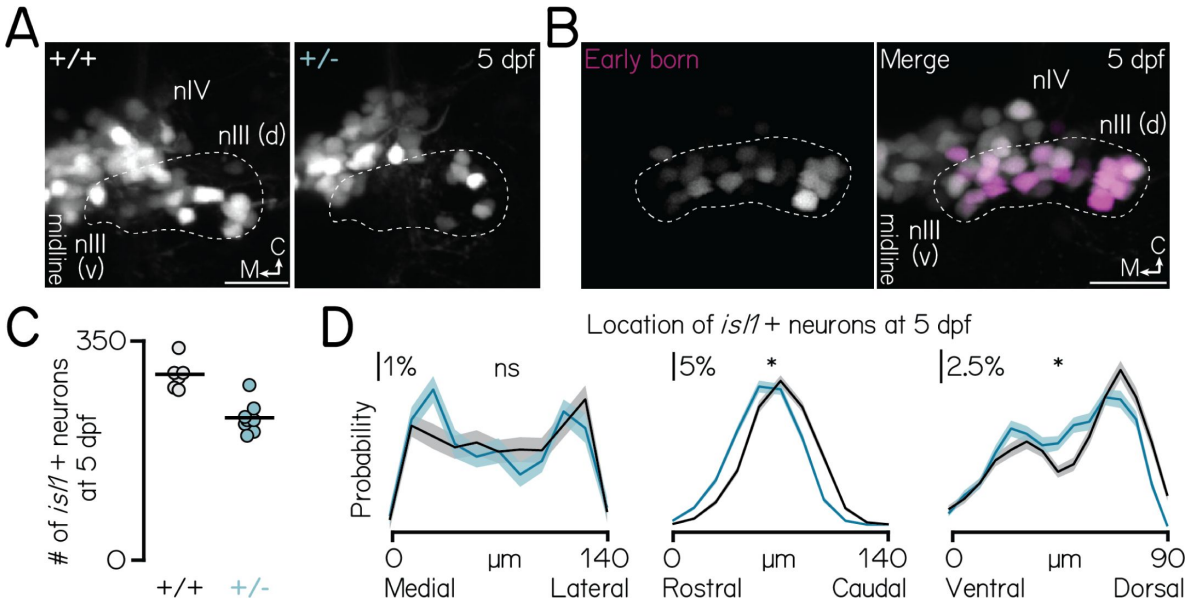

Figure S1

phox2a specifies nIII motor neuron fate in a dose- and birthdate-dependent manner.

Associated with **Figure 1**.
(A) Images of nIII/nIV motor neurons, labeled in *Tg(isl1:GFP)*, in wildtype siblings (left) and *phox2a* heterozygotes (middle) at 5 dpf. Wildtype image same as in **Figure 1E**. One hemisphere shown. White dashed lines outline the dorsal extent of nIII, which contains inferior rectus and medial rectus neurons [33]. Scale bar, 20 μm.
(B) Location of the earliest-born neurons in nIII/nIV (left, magenta) against all nIII/nIV neurons labeled in *Tg(isl1:Kaede)* (right, grey). Larvae birthdated at 34 hpf (Methods). One hemisphere shown. White dashed lines outline the dorsal extent of nIII. Scale bar, 20 μm.
(C) Quantification of the number of *Tg(isl1:GFP)*+ neurons in nIII/nIV from N=6 wildtype siblings (grey) and N=8 *phox2a* heterozygotes (teal). Wildtype data same as **Figure 1F**.
(D) Distributions showing probability of nIII/nIV soma location across each spatial axis in wildtype (black) and heterozygous (teal) *phox2a* larvae. Solid and shaded lines show mean and standard deviation, respectively, from bootstrapped data. Data from same fish quantified in **Figure S1C**. ns, not significant; star, significant at the p<0.001 level.

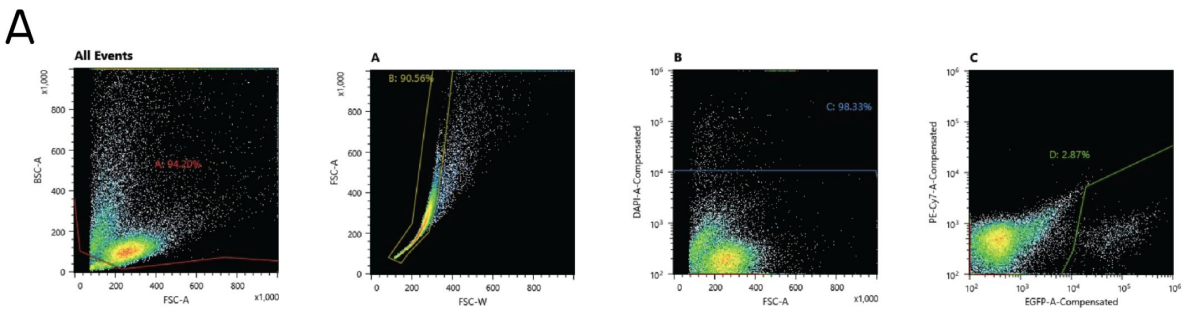

Figure S2

Flow cytometry gating strategy to sort fluorescently-labeled neurons for bulk RNA sequencing.

Associated with **Figure 5**.
(A) Sequential gates used to sort fluorescent neurons labeled with *Tg(-6.7Tru.Hcrtr2:GAL4-VP16);Tg(UAS-E1b:Kaede);Tg(isl1:GFP)*. Gate A excluded presumptive debris (small cells). Gate B isolated single cells and excluded large cells and doublets. Gate C excluded DAPI+ (dead or unhealthy) neurons. Gate D isolated fluorescent (GFP or Kaede+) neurons; neurons in this gate were sorted. Gates were set using negative controls (not shown; Methods). Gates shown for one of four experimental repeats.

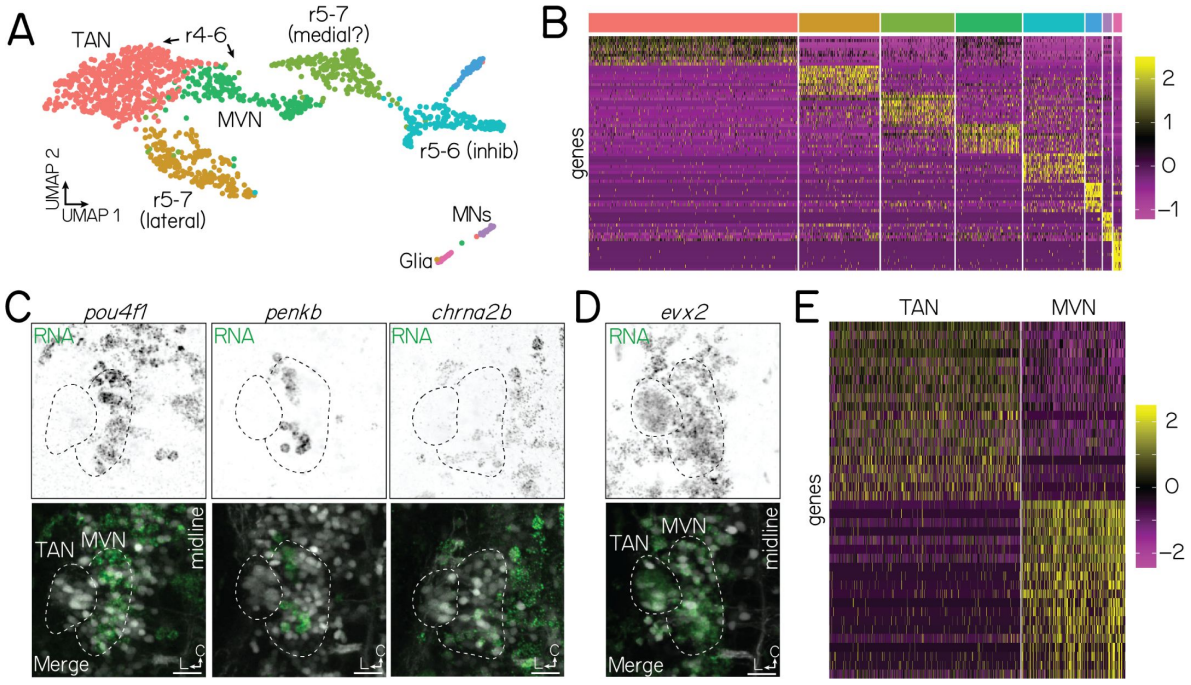

Figure S3

Molecular identification of projection neurons using a reference single-cell RNA sequencing atlas.

Associated with **Figure 5**.

(A) UMAP visualization of a single-cell RNA sequencing atlas of n=1,468 neurons labeled in *Tg(-6.7Tru.Hcrtr2:GAL4-VP16);Tg(UAS-E1b:Kaede)*, generated with 10x Genomics (Methods). Each circle is a single neuron. Neurons are clustered (colors) according to their transcriptional identity. Annotations are based on validated marker genes (data not shown). TAN, tangential nucleus; MVN, medial vestibular nucleus; r, rhombomere; MNs, motor neurons; inhib, inhibitory neurons.

(B) Heatmap showing genes unique to each annotated cluster. Each row is a gene; names unlisted for clarity. Columns show distinct clusters. Color bar on top reflects clusters in **Figure S3A**. Yellow and purple reflect stronger or weaker gene expression, respectively.

(C) Fluorescent *in situ* hybridization against three markers (*pou4f1, penkb, chrna2b*) that are negative for tangential nucleus projection neurons and positive for medial vestibular nucleus neurons. Top row shows RNA expression (green); bottom row, merge with neurons labeled in *Tg(-6.7Tru.Hcrtr2:GAL4-VP16);Tg(UAS-E1b:Kaede)*. Dashed lines outline the tangential nucleus (TAN) and medial vestibular nucleus (MVN). Data from 72 hpf larvae. Images shown in an axial view.

(D) Fluorescent *in situ* hybridization against a positive marker (*evx2*) for both tangential nucleus and medial vestibular nucleus neurons. All scale bars, 20 µm.

(E) Heatmap showing genes unique to tangential and medial vestibular neurons. Clusters identified using positive and negative fluorescent *in situ* data from **Figure S3C**-**Figure S3D** and unpublished data.

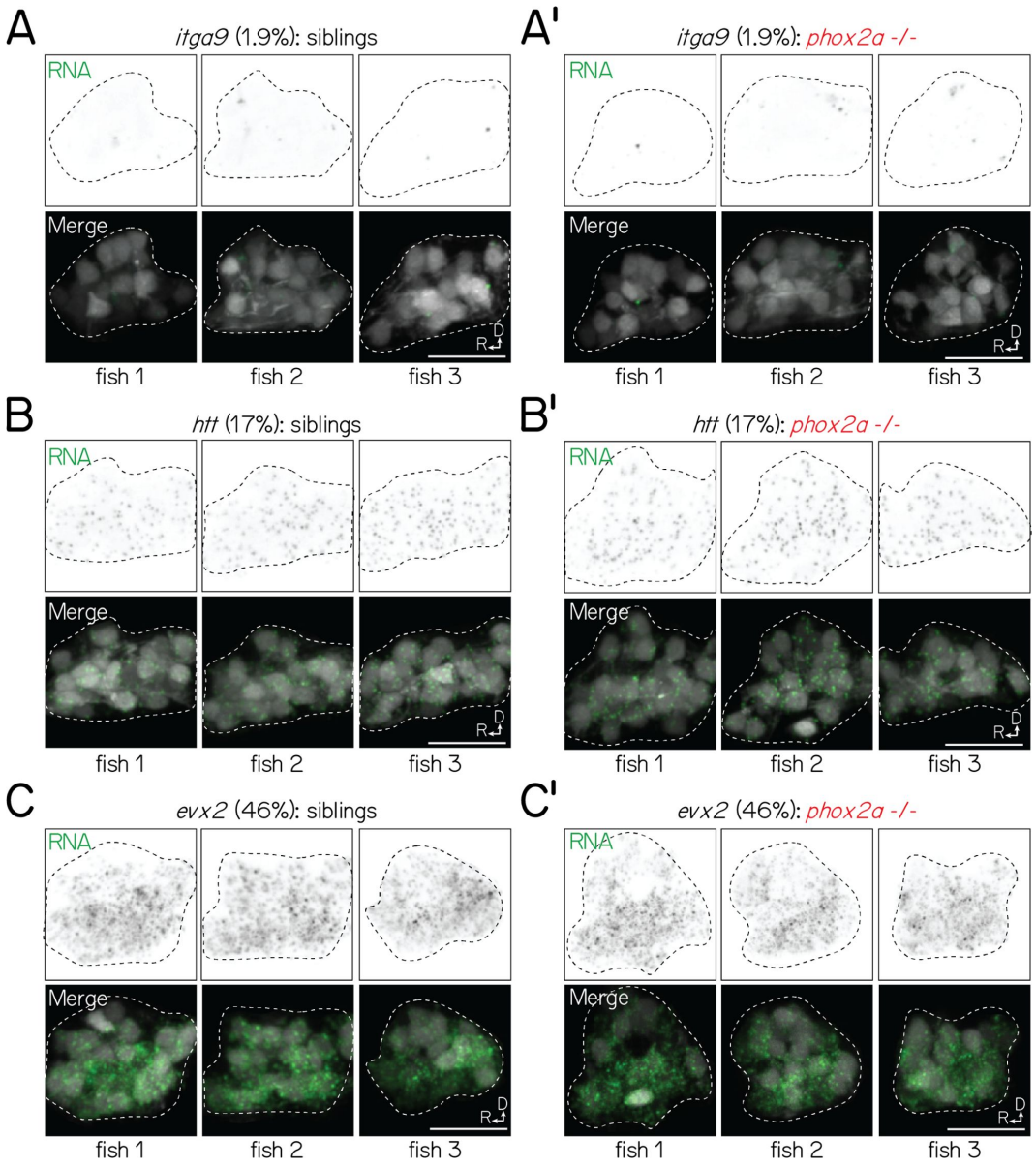

Figure S4

Visualization of transcripts in siblings and *phox2a* null mutants with fluorescent *in situ* hybridization is (1) consistent across larvae and (2) scales with predicted detection in projection neurons.

Associated with **Figure 5**.

(A-A') Fluorescent *in situ* hybridization against *itga9* for three sibling (A) or *phox2a* null mutant (A') larvae (72 hpf), imaged with identical conditions. Left column shows RNA (green); right column, merge with projection neurons visualized with *Tg(-6.7Tru.Hcrtr2:GAL4-VP16);Tg(UAS-E1b:Kaede)* (grey). Dashed lines outline the projection nucleus. Cell and transcript expression outside the projection nucleus is removed for visual clarity. Percentage (1.9%) refers to fraction of cells in a single-cell RNA sequencing reference atlas (Methods) with detected transcript. All scale bars, 20 μm.

(B-B') Fluorescent *in situ* hybridization against *htt*, 17%, for three sibling (B) and *phox2a* mutant (B') larvae (72 hpf).

(C-C') Fluorescent *in situ* hybridization against *evx2*, 46%, for three sibling (C) and *phox2a* mutant (C') larvae (72 hpf).

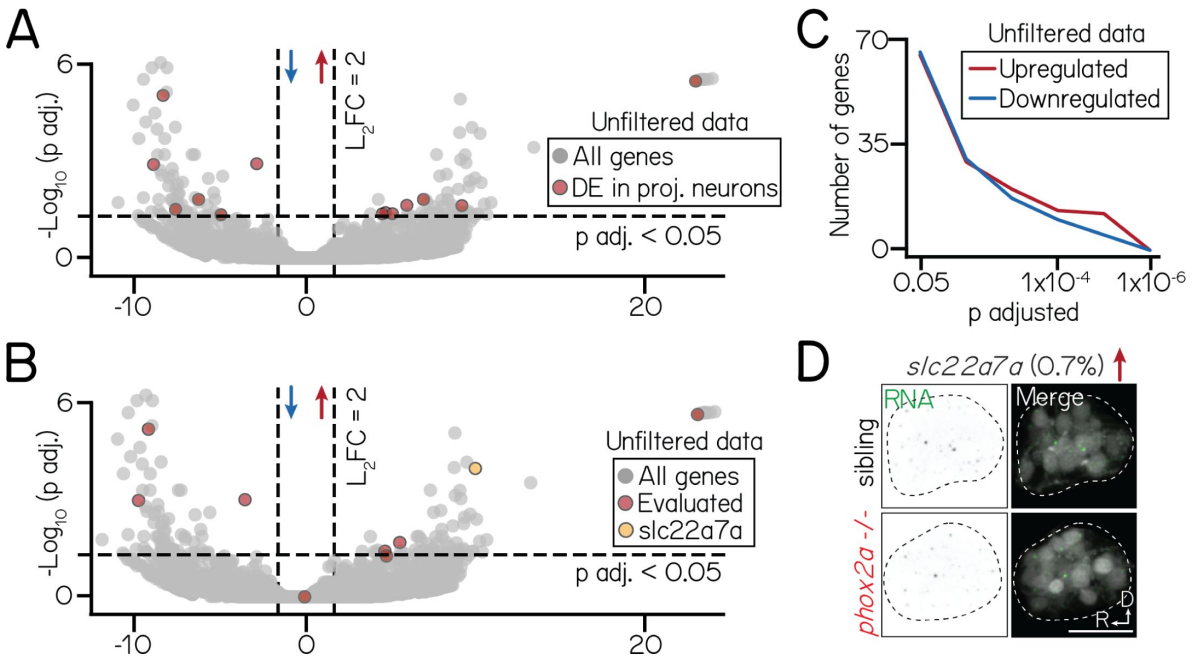

Figure S5

Differential gene expression in an unfiltered bulk sequencing dataset of siblings and *phox2a* mutants.

Associated with **Figure 5**.

(A) Volcano plot showing differentially expressed genes across an unfiltered bulk RNA sequencing dataset. Dashed lines represent significance cutoffs: horizontal line, p adjusted>0.05; vertical line, Log_2 Fold Change > 2.0. Each circle is a gene. Genes to the left and right of 0 on the horizontal axis show downregulated and upregulated genes, respectively. Red color shows genes that are differentially expressed in a filtered subset of projection neurons (**Figure 5**). Grey-colored genes are below both significance thresholds.

(B) Same data as **Figure S5A**, now highlighting candidate genes evaluated by fluorescent *in situ* (**Figure 5**) with red. One candidate (yellow) that did not meet projection neuron filter criteria (Methods) is shown in **Figure S5D**; remaining candidates (included in filtered data) shown in **Figure 5F**.

(C) Same data as **Figure S5A**-**Figure S5B**, showing the number of differentially expressed genes at progressive significance thresholds (p adjusted). Red and blue lines show the number of significantly upregulated and downregulated genes, respectively.

(D) Fluorescent *in situ* hybridization against a candidate gene, *slc22a7a* (log_2 fold change=10.2, p adj.=1.6×10^{-4}), that did not meet projection neuron filter criteria. Percentage refers to fraction of projection neurons from a single-cell sequencing dataset with expression (Methods). Left columns show RNA (green); right columns, merge with projection neurons labeled with *Tg(-6.7Tru.Hcrtr2:GAL4-VP16);Tg(UAS-E1b:Kaede)* (grey). Dashed lines outline the projection nucleus. Cell and transcript expression outside the projection nucleus is removed for visual clarity. All scale bars, 20 µm.

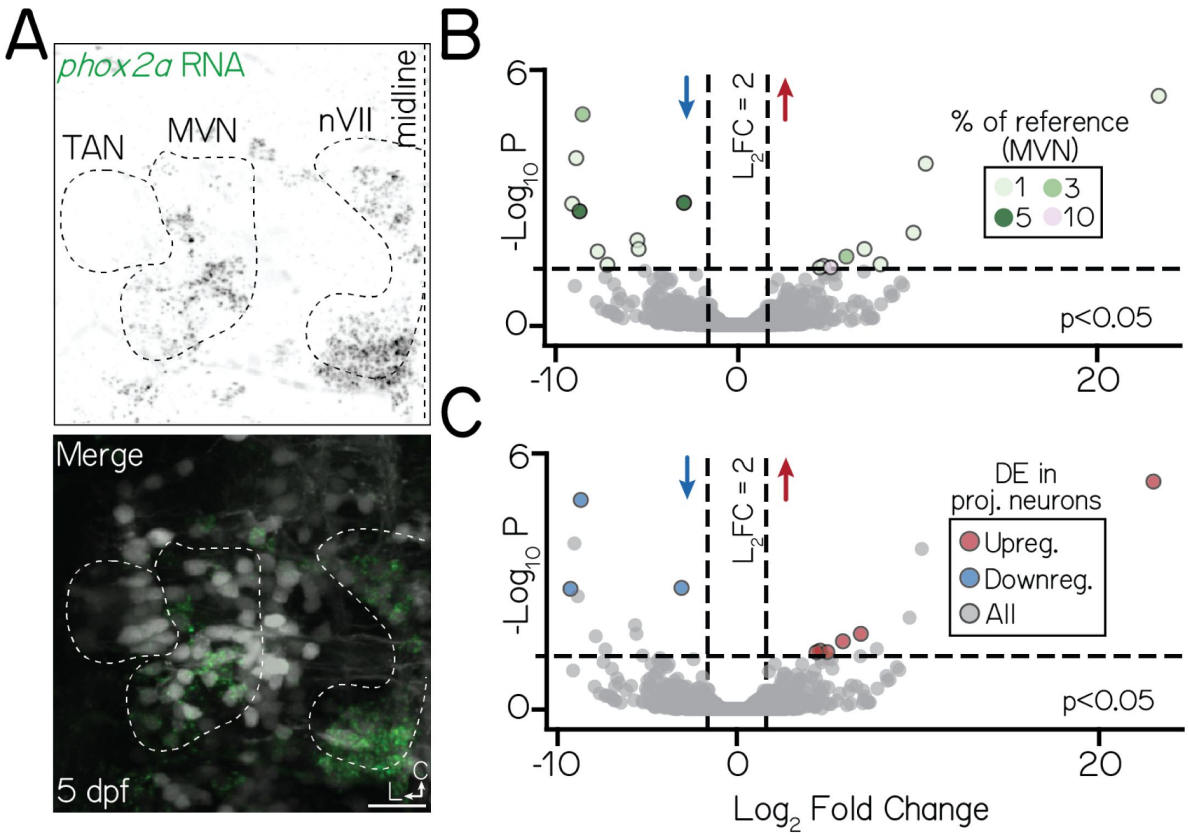

Figure S6

phox2a expression in the medial vestibular nucleus may underscore differential gene expression phenotypes in bulk data.

Associated with **Figure 5**.

(A) Fluorescent *in situ* hybridization against *phox2a* in a 5 dpf larvae (axial view). Top panel shows *phox2a* RNA (green); bottom panel, merge with neurons visualized with *Tg(isl1:GFP)*;*Tg(-6.7Tru.Hcrtr2:GAL4-VP16(*;*Tg(UAS-E1b:Kaede)* (grey). White dashed lines outline three nuclei of interest: projection neurons in the tangential nucleus (TAN), the medial vestibular nucleus (MVN), and the facial nucleus (nVII). All scale bars, 20 µm.

(B) Volanco plot showing differentially expressed genes in medial vestibular nucleus neurons between control and *phox2a* null larvae at 3 dpf. Dashed lines represent significance cutoffs: horizontal line, p>0.05; vertical line, Log_2 Fold Change > 2.0. Each circle is a gene. Genes to the left and right of 0 on the horizontal axis show downregulated and upregulated genes, respectively. Colors indicate percent of reference medial vestibular neurons (Methods) that express a given gene. Grey-colored genes are below both significance thresholds.

(C) Same data as **Figure S6B**. Color shows genes that are differentially expressed in both medial vestibular nucleus neurons and projection neurons.

References

1. Sherrington Charles S. (1906) **The Integrative Action of the Nervous System**

2. Matise Michael P., Lance-Jones Cynthia (1996) **A critical period for the specification of motor pools in the chick lumbosacral spinal cord** *Development* **122**

3. Glover Joel C. (2003) **The development of vestibulo-ocular circuitry in the chicken embryo** *Journal of Physiology-Paris* **97**:17–25

4. Arber Silvia (2012) **Motor circuits in action: Specification, connectivity, and function** *Neuron* **74**:975–989

5. Dasen Jeremy S (2017) **Master or servant? emerging roles for motor neuron subtypes in the construction and evolution of locomotor circuits** *Current Opinion in Neurobiology* **42**:25–32

6. Ladle David R., Pecho-Vrieseling Eline, Arber Silvia (2007) **Assembly of motor circuits in the spinal cord: Driven to function by genetic and experience-dependent mechanisms** *Neuron* **56**:270–283

7. Machado Timothy A., Pnevmatikakis Eftychios, Paninski Liam, Jessell Thomas M., Miri Andrew (2015) **Primacy of flexor locomotor pattern revealed by ancestral reversion of motor neuron identity** *Cell* **162**

8. Hinckley Christopher A., Alaynick William A., Gallarda Benjamin W., Hayashi Marito, Hilde Kathryn L., Driscoll Shawn P., Dekker Joseph D., Tucker Haley O., Sharpee Tatyana O., Pfaff Samuel L. (2015) **Spinal locomotor circuits develop using hierarchical rules based on motorneuron position and identity** *Neuron* **87**:1008–1021

9. Vrieseling Eline, Arber Silvia (2006) **Target-induced transcriptional control of dendritic patterning and connectivity in motor neurons by the ETS gene pea3** *Cell* **127**:1439–1452

10. Baek Myungin, Pivetta Chiara, Liu Jeh-Ping, Arber Silvia, Dasen Jeremy S. (2017) **Columnar-intrinsic cues shape premotor input specificity in locomotor circuits** *Cell Reports* **21**:867–877

11. Balaskas Nikolaos, Abbott L.F., Jessell Thomas M., Ng David (2019) **Positional strategies for connection specificity and synaptic organization in spinal sensory-motor circuits** *Neuron* **102**:1143–1156

12. Wang Guoying, Scott Sheryl A. (2000) **The waiting period of sensory and motor axons in early chick hindlimb: Its role in axon pathfinding and neuronal maturation** *The Journal of Neuroscience* **20**

13. Sürmeli Gülşen, Akay Turgay, Ippolito Gregory C., Tucker Philip W., Jessell Thomas M. (2011) **Patterns of spinal sensory-motor connectivity prescribed by a dorsoventral positional template** *Cell* **147**:653–665

14. Bikoff Jay B. *et al.* (2016) **Spinal inhibitory interneuron diversity delineates variant motor microcircuits** *Cell* **165**:207–219

15. Sweeney Lora B., Bikoff Jay B., Gabitto Mariano I., Brenner-Morton Susan, Baek Myungin, Yang Jerry H., Tabak Esteban G., Dasen Jeremy S., Kintner Christopher R., Jessell Thomas M. (2018) **Origin and segmental diversity of spinal inhibitory interneurons** *Neuron* **97**:341–355

16. Shin Maggie M, Catela Catarina, Dasen Jeremy (2020) **Intrinsic control of neuronal diversity and synaptic specificity in a proprioceptive circuit** *eLife* **9**

17. Kiehn Ole (2016) **Decoding the organization of spinal circuits that control locomotion** *Nature Reviews Neuroscience* **17**

18. Hunt J. Ramsay (1923) **The dual nature of the efferent nervous system: A further study of the static and kinetic systems, their function and symptomatology contents** *Archives of Neurology & Psychiatry* **10**

19. Sharma Kamal, Sheng Hui Z, Lettieri Karen, Li Hung, Karavanov Alexander, Potter Steven, Westphal Heiner, Pfaff Samuel L (1998) **Lim homeodomain factors lhx3 and lhx4 assign subtype identities for motor neurons** *Cell* **95**

20. Hutchinson Sarah A., Eisen Judith S. (2006) **Islet1 and islet2 have equivalent abilities to promote motoneuron formation and to specify motoneuron subtype identity** *Development* **133**

21. Szentágothai J. (1964) **Pathways and synaptic articulation patterns connecting vestibular receptors and oculomotor nuclei** *The Oculomotor System* :205–223

22. Straka Hans, Baker Robert, Gilland Edwin (2001) **Rhombomeric organization of vestibular pathways in larval frogs** *Journal of Comparative Neurology* **437**:42–55

23. Díaz Carmen, Glover Joel C., Puelles Luis, Bjaalie Jan G. (2003) **The relationship between hodological and cytoarchitectonic organization in the vestibular complex of the 11-day chicken embryo** *The Journal of Comparative Neurology* **457**:87–105

24. Bianco Isaac H., Ma Leung-Hang, Schoppik David, Robson Drew N., Orger Michael B., Beck James C., Li Jennifer M., Schier Alexander F., Engert Florian, Baker Robert (2012) **The tangential nucleus controls a gravito-inertial vestibulo-ocular reflex** *Current Biology* **22**:1285–1295

25. Schoppik David, Bianco Isaac H., Prober David A., Douglass Adam D., Robson Drew N., Li Jennifer M.B., Greenwood Joel S.F., Soucy Edward, Engert Florian, Schier Alexander F. (2017) **Gaze-stabilizing central vestibular neurons project asymmetrically to extraocular motoneuron pools** *The Journal of Neuroscience* **37**:11353–11365

26. Bagnall Martha W, Schoppik David (2018) **Development of vestibular behaviors in zebrafish** *Current Opinion in Neurobiology* **53**:83–89

27. Díaz Carmen, Puelles Luis (2018) **Segmental analysis of the vestibular nerve and the efferents of the vestibular complex** *The Anatomical Record* **302**:472–484

28. Liu Zhikai, Hildebrand David G. C., Morgan Joshua L., Jia Yizhen, Slimmon Nicholas, Bagnall Martha W. (2022) **Organization of the gravity-sensing system in zebrafish** *Nature Communications* **13**

29. Goldblatt Dena *et al.* (2023) **Neuronal birthdate reveals topography in a vestibular brainstem circuit for gaze stabilization** *Current Biology* **33**:1265–1281

30. Glover Joel C. (2000) **Neuroepithelial 'compartments' and the specification of vestibular projections** *Progress in Brain Research* :3–21

31. Straka Hans (2010) **Ontogenetic rules and constraints of vestibulo-ocular reflex development** *Current Opinion in Neurobiology* **20**:689–695

32. Clark C., Austen O., Poparic I., Guthrie S. (2013) **α2-chimaerin regulates a key axon guidance transition during development of the oculomotor projection** *Journal of Neuroscience* **33**:16540–16551

33. Greaney Marie R., Privorotskiy Ann E., D'Elia Kristen P., Schoppik David (2016) **Extraocular motoneuron pools develop along a dorsoventral axis in zebrafish, Danio rerio** *Journal of Comparative Neurology* **525**:65–78

34. Guo Su, Brush Jennifer, Teraoka Hiroki, Goddard Audrey, Wilson Stephen W., Mullins Mary C., Rosenthal Arnon (1999) **Development of noradrenergic neurons in the zebrafish hindbrain requires BMP, FGF8, and the homeodomain protein soulless/phox2a** *Neuron* **24**:555–566

35. Coppola Eva, Pattyn Alexandre, Guthrie Sarah C, Goridis Christo, Studer Michèle (2005) **Reciprocal gene replacements reveal unique functions for phox2 genes during neural differentiation** *The EMBO Journal* **24**

36. Hasan K. B., Agarwala S., Ragsdale C. W. (2010) **PHOX2a regulation of oculomotor complex nucleogenesis** *Development* **137**:1205–1213

37. Nakano Motoi, Yamada Koki, Fain Jennifer, Sener Emin C., Selleck Carol J., Awad Abdulaziz H., Zwaan Johan, Mullaney Paul B., Bosley Thomas M., Engle Elizabeth C. (2001) **Homozygous mutations in arix(phox2a) result in congenital fibrosis of the extraocular muscles type 2** *Nature Genetics* **29**

38. Bosley Thomas M., Oystreck Darren T., Robertson Richard L., al Awad Abdulaziz, Abu-Amero Khaled, Engle Elizabeth C. (2006) **Neurological features of congenital fibrosis of the extraocular muscles type 2 with mutations in PHOX2a** *Brain* **129**:2363–2374

39. Varela-Echavarria Alfredo, Pfaff Samuel L., Guthrie Sarah (1996) **Differential expression of LIM homeobox genes among motor neuron subpopulations in the developing chick brain stem** *Molecular and Cellular Neuroscience* **8**:242–257

40. Higashijima S., Hotta Y., Okamoto H. (2000) **Visualization of cranial motor neurons in live transgenic zebrafish expressing green fluorescent protein under the control of the Islet-1 promoter/enhancer** *Journal of Neuroscience* **20**:206–218

41. Hamling Kyla R., Zhu Yunlu, Auer Franziska, Schoppik David (2023) **Tilt in place microscopy: a simple, low-cost solution to image neural responses to body rotations** *The Journal of Neuroscience* **43**

42. Chen Tsai-Wen *et al.* (2013) **Ultrasensitive fluorescent proteins for imaging neuronal activity** *Nature* **499**:295–300

43. Evinger Craig (1988) **Extraocular motor nuclei: location, morphology and afferents** *Reviews of Oculomotor Research* **2**:81–117

44. Pujala Avinash, Koyama Minoru (2019) **Chronology-based architecture of descending circuits that underlie the development of locomotor repertoire after birth** *eLife* **8**

45. Dalva Matthew B., McClelland Andrew C., Kayser Matthew S. (2007) **Cell adhesion molecules: signalling functions at the synapse** *Nature Reviews Neuroscience* **8**

46. Moreland Trevor, Poulain Fabienne E. (2022) **To stick or not to stick: The multiple roles of cell adhesion molecules in neural circuit assembly** *Frontiers in Neuroscience* **16**

47. DElia Kristen P. *et al.* (2023) **Determinants of motor neuron functional subtypes important for locomotor speed** *Cell Reports* **42**

48. Scott Ethan K., Mason Lindsay, Arrenberg Aristides B., Ziv Limor, Gosse Nathan J, Xiao Tong, Chi Neil C., Asakawa Kazuhide, Kawakami Koichi, Baier Herwig (2007) **Targeting neural circuitry in zebrafish using GAL4 enhancer trapping** *Nature Methods*

49. Lacoste Alix M.B., Schoppik David, Robson Drew N., Haesemeyer Martin, Portugues Ruben, Li Jennifer M., Randlett Owen, Wee Caroline L., Engert Florian, Schier Alexander F. (2015) **A convergent and essential interneuron pathway for mauthner-cell-mediated escapes** *Current Biology* **25**:1526–1534

50. Sugioka Takumi, Tanimoto Masashi, Higashijima Shin-ichi (2023) **Biomechanics and neural circuits for vestibular-induced fine postural control in larval zebrafish** *Nature Communications* **14**

51. Choi Harry M. T., Schwarzkopf Maayan, Fornace Mark E., Acharya Aneesh, Artavanis Georgios, Stegmaier Johannes, Cunha Alexandre, Pierce Niles A. (2018) **Third-generation in situ hybridization chain reaction: multiplexed, quantitative, sensitive, versatile, robust** *Development* **145**

52. Rodney P (2000) **DeKoter and Harinder Singh. Regulation of b lymphocyte and macrophage development by graded expression of pu.1** *Science* **288**

53. Liu Zijing, Hu Xuemei, Cai Jun, Liu Ben, Peng Xiaozhong, Wegner Michael, Qiu Mengsheng (2007) **Induction of oligodendrocyte differentiation by olig2 and sox10: Evidence for reciprocal interactions and dosage-dependent mechanisms** *Developmental Biology* **302**

54. Sansom Stephen N., Griffiths Dean S., Faedo Andrea, Kleinjan Dirk-Jan, Ruan Youlin, Smith James, van Heyningen Veronica, Rubenstein John L., Livesey Frederick J. (2009) **The level of the transcription factor pax6 is essential for controlling the balance between neural stem cell self-renewal and neurogenesis** *PLoS Genetics* **5**

55. Vemaraju Shruti, Kantarci Husniye, Padanad Mahesh S., Riley Bruce B. (2012) **A spatial and temporal gradient of fgf differentially regulates distinct stages of neural development in the zebrafish inner ear** *PLoS Genetics* **8**

56. Komiyama Takaki, Sweeney Lora B., Schuldiner Oren, Christopher Garcia K., Luo Liqun (2007) **Graded expression of semaphorin-1a cell-autonomously directs dendritic targeting of olfactory projection neurons** *Cell* **128**

57. Park Jong G. *et al.* (2016) **Loss of mafb function in humans and mice causes duane syndrome, aberrant extraocular muscle innervation, and inner-ear defects** *The American Journal of Human Genetics* **98**

58. Cheng Long *et al.* (2014) **Human cfeom1 mutations attenuate kif21a autoinhibition and cause oculomotor axon stalling** *Neuron* **82**

59. Cederquist Gustav Y. *et al.* (2012) **An inherited tubb2b mutation alters a kinesin-binding site and causes polymicrogyria, cfeom and axon dysinnervation** *Human Molecular Genetics* **21**

60. Evinger Craig, Graf Werner M., Baker Robert (1987) **Extra- and intracellular HRP analysis of the organization of extraocular motoneurons and internuclear neurons in the guinea pig and rabbit** *The Journal of Comparative Neurology* **262**:429–445

61. Knüfer Athene, Diana Giovanni, Walsh Gregory S, Clarke Jonathan DW, Guthrie Sarah (2020) **Cadherins regulate nuclear topography and function of developing ocular motor circuitry** *eLife* **9**

62. Lin Jonathan H, Saito Tetsuichiro, Anderson David J, Lance-Jones Cynthia, Jessell Thomas M, Arber Silvia (1998) **Functionally related motor neuron pool and muscle sensory afferent subtypes defined by coordinate ets gene expression** *Cell* **95**

63. Dasen Jeremy S., Tice Bonnie C., Brenner-Morton Susan, Jessell Thomas M. (2005) **A hox regulatory network establishes motor neuron pool identity and target-muscle connectivity** *Cell* **123**:477–491

64. Dasen Jeremy S., De Camilli Alessandro, Wang Bin, Tucker Philip W., Jessell Thomas M. (2008) **Hox repertoires for motor neuron diversity and connectivity gated by a single accessory factor, FoxP1** *Cell* **134**:304–316

65. Hanley Olivia, Zewdu Rediet, Cohen Lisa J., Jung Heekyung, Lacombe Julie, Philippidou Polyxeni, Lee David H., Selleri Licia, Dasen Jeremy S. (2016) **Parallel pbx -dependent pathways govern the coalescence and fate of motor columns** *Neuron* **91**:1005–1020

66. Philippidou Polyxeni, Dasen JeremyăS. (2013) **Hox genes: Choreographers in neural development, architects of circuit organization** *Neuron* **80**

67. Whitman Mary C., Engle Elizabeth C. (2022) **Genetics of Strabismus**

68. Supèr Hans, Martnez Albert, Del Ro José A., Soriano Eduardo (1998) **Involvement of distinct pioneer neurons in the formation of layer-specific connections in the hippocampus** *The Journal of Neuroscience* **18**

69. McConnell Susan K., Ghosh Anirvan, Shatz Carla J. (1989) **Subplate neurons pioneer the first axon pathway from the cerebral cortex** *Science* **245**

70. Bentley David, Keshishian Haig (1982) **Pathfinding by peripheral pioneer neurons in grasshoppers** *Science* **218**

71. Bate C. M. (1976) **Pioneer neurones in an insect embryo** *Nature* **260**

72. Pike Susan H., Melancon Eloine F., Eisen Judith S. (1992) **Pathfinding by zebrafish motoneurons in the absence of normal pioneer axons** *Development* **114**

73. Landmesser Lynn, Honig Marcia G. (1986) **Altered sensory projections in the chick hind limb following the early removal of motoneurons** *Developmental Biology* **118**

74. Scott Sheryl A. (1988) **Skin sensory innervation patterns in embryonic chick hindlimbs deprived of motoneurons** *Developmental Biology* **126**

75. Swanson Gavin J., Lewis Julian (1986) **Sensory nerve routes in chick wing buds deprived of motor innervation** *Development* **95**

76. Tosney Kathryn W., Hageman Martha S. (1989) **Different subsets of axonal guidance cues are essential for sensory neurite outgrowth to cutaneous and muscle targets in the dorsal ramus of the embryonic chick** *Journal of Experimental Zoology* **251**

77. Whitlock Kathleen E., Westerfield Monte (1998) **A transient population of neurons pioneers the olfactory pathway in the zebrafish** *The Journal of Neuroscience* **18**

78. Easter Jr S. S., Nicola G. N. (1997) **The development of eye movements in the zebrafish (Danio rerio)** *Developmental psychobiology* **31**:267–276

79. Noden D. M., Marcucio R., Borycki A., Emerson Jr C. P. (1999) **Differentiation of avian craniofacial muscles: I. patterns of early regulatory gene expression and myosin heavy chain synthesis** *Developmental Dynamics* **216**:96–112

80. McCrea R. A., Strassman A., Highstein S. M. (1987) **Anatomical and physiological characteristics of vestibular neurons mediating the vertical vestibulo-ocular reflexes of the squirrel monkey** *The Journal of Comparative Neurology* **264**:571–594

81. Mendelson Bruce (1986) **Development of reticulospinal neurons of the zebrafish. ii. early axonal outgrowth and cell body position** *Journal of Comparative Neurology* **251**

82. Severi Kristen E., Portugues Ruben, Marques João C., O'Malley Donald M., Orger Michael B., Engert Florian (2014) **Neural control and modulation of swimming speed in the larval zebrafish** *Neuron* **83**:692–707

83. Thiele Tod R., Donovan Joseph C., Baier Herwig (2014) **Descending control of swim posture by a midbrain nucleus in zebrafish** *Neuron* **83**:679–691

84. Wang Wei-Chun, McLean David L. (2014) **Selective responses to tonic descending commands by temporal summation in a spinal motor pool** *Neuron* **83**:708–721

85. Tanimoto Masashi, Watakabe Ikuko, Higashijima Shin ichi (2022) **Tiltable objective microscope visualizes discrimination of static and dynamic head movement originates at hair cells** *bioRxiv*

86. Berg Eva M., Mrowka Leander, Bertuzzi Maria, Madrid David, Picton Laurence D., Manira Abdeljabbar El (2023) **Brainstem circuits encoding start, speed, and duration of swimming in adult zebrafish** *Neuron* **111**:372–386

87. Yamagata Masahito, Weiner Joshua A., Sanes Joshua R. (2002) **Sidekicks** *Cell* **110**

88. Yamagata Masahito, Sanes Joshua R. (2008) **Dscam and sidekick proteins direct lamina-specific synaptic connections in vertebrate retina** *Nature* **451**

89. Arber Silvia, Ladle David R, Lin Jonathan H, Frank Eric, Jessell Thomas M (2000) **Ets gene er81 controls the formation of functional connections between group ia sensory afferents and motor neurons** *Cell* **101**

90. Pecho-Vrieseling Eline, Sigrist Markus, Yoshida Yutaka, Jessell Thomas M., Arber Silvia (2009) **Specificity of sensory–motor connections encoded by sema3e–plxnd1 recognition** *Nature* **459**:842–846

91. Bonanomi D., Pfaff S. L. (2010) **Motor axon pathfinding** *Cold Spring Harbor Perspectives in Biology* **2**

92. Duan Xin, Krishnaswamy Arjun, DeălaăHuerta Irina, Sanes JoshuaăR. (2014) **Type ii cadherins guide assembly of a direction-selective retinal circuit** *Cell* **158**

93. Al-Khindi Timour, Sherman Michael B., Kodama Takashi, Gopal Preethi, Pan Zhiwei, Kiraly James K., Zhang Hao, Goff Loyal A., du Lac Sascha, Kolodkin Alex L. (2022) **The transcription factor tbx5 regulates direction-selective retinal ganglion cell development and image stabilization** *Current Biology*

94. Kurmangaliyev Yerbol Z, Yoo Juyoun, LoCascio Samuel A, Lawrence Zipursky S (2019) **Modular transcriptional programs separately define axon and dendrite connectivity** *eLife* **8**

95. Yoo Juyoun, Dombrovski Mark, Mirshahidi Parmis, Nern Aljoscha, LoCascio Samuel A., Lawrence Zipursky S., Kurmangaliyev Yerbol Z. (2023) **Brain wiring determinants uncovered by integrating connectomes and transcriptomes** *Current Biology* **33**:3998–4005

96. Dasen Jeremy S. (2009) **Chapter 4 Transcriptional Networks in the Early Development of SensoryMotor Circuits**

97. Sharma Nikhil, Flaherty Kali, Lezgiyeva Karina, Wagner Daniel E., Klein Allon M., Ginty David D. (2020) **The emergence of transcriptional identity in somatosensory neurons** *Nature* **577**

98. Shrestha Brikha R., Chia Chester, Wu Lorna, Kujawa Sharon G., Charles Liberman M., Goodrich Lisa V. (2018) **Sensory neuron diversity in the inner ear is shaped by activity** *Cell* **174**:1229–1246

99. Alaynick William A., Jessell Thomas M., Pfaff Samuel L. (2011) **Snapshot: Spinal cord development** *Cell* **146**:178–178

100. Tessier-Lavigne Marc, Goodman Corey S. (1996) **The molecular biology of axon guidance** *Science* **274**

101. Goodman Corey S., Shatz Carla J. (1993) **Developmental mechanisms that generate precise patterns of neuronal connectivity** *Cell* **72**

102. Spead Olivia, Moreland Trevor, Weaver Cory J., Costa Irene Dalla, Hegarty Brianna, Kramer Kenneth L., Poulain Fabienne E. (2023) **Teneurin trans-axonal signaling prunes topographically missorted axons** *Cell Reports* **42**

103. Zecca A., Dyballa S., Voltes A., Bradley R., Pujades C. (2015) **The order and place of neuronal differentiation establish the topography of sensory projections and the entry points within the hindbrain** *Journal of Neuroscience* **35**:7475–7486

104. Dyballa Sylvia, Savy Thierry, Germann Philipp, Mikula Karol, Remesikova Mariana, Špir Róbert, Zecca Andrea, Peyriéras Nadine, Pujades Cristina (2017) **Distribution of neurosensory progenitor pools during inner ear morphogenesis unveiled by cell lineage reconstruction** *eLife* **6**

105. Fritzsch B., Nichols D.H. (1993) **Dii reveals a prenatal arrival of efferents at the differentiating otocyst of mice** *Hearing Research* **65**

106. Altman Joseph, Bayer Shirley A. (1982) **Development of the Cranial Nerve Ganglia and Related Nuclei in the Rat**

107. McConnell Jo Ann, Sechrist John W. (1980) **Identification of early neurons in the brainstem and spinal cord: I. an autoradiographic study in the chick** *Journal of Comparative Neurology* **192**

108. Maklad Adel, Fritzsch Bernd (2003) **Development of vestibular afferent projections into the hindbrain and their central targets** *Brain Research Bulletin* **60**

109. Auclair Franois, Marchand Raymond, Glover Joel C. (1999) **Regional patterning of reticulospinal and vestibulospinal neurons in the hindbrain of mouse and rat embryos** *The Journal of Comparative Neurology* **411**

110. Altman Joseph, Bayer Shirley A. (1981) **Development of the brain stem in the rat. V. Thymidine-radiographic study of the time of origin of neurons in the midbrain tegmentum** *The Journal of Comparative Neurology* **198**:677–716

111. Shaw Marjorie D., Alley Keith E. (1981) **Generation of the ocular motor nuclei and their cell types in the rabbit** *The Journal of Comparative Neurology* **200**:69–82

112. Puelles Luis, Privat Alain (1977) **Do oculomotor neuroblasts migrate across the midline in the fetal rat brain?** *Anatomy and Embryology* **150**

113. Moens Cecilia B., Prince Victoria E. (2002) **Constructing the hindbrain: Insights from the zebrafish** *Developmental Dynamics* **224**:1–17

114. Kinkhabwala Amina, Riley Michael, Koyama Minoru, Monen Joost, Satou Chie, Kimura Yukiko, Higashijima Shin ichi, Fetcho Joseph (2011) **A structural and functional ground plan for neurons in the hindbrain of zebrafish** *Proceedings of the National Academy of Sciences* **108**:1164–1169

115. Farnsworth Dylan R., Saunders Lauren M., Miller Adam C. (2020) **A single-cell transcriptome atlas for zebrafish development** *Developmental Biology* **459**:100–108

116. Tambalo Monica, Mitter Richard, Wilkinson David G. (2020) **A single cell transcriptome atlas of the developing zebrafish hindbrain** *Development*

117. Ferrario Juan E., Baskaran Pranetha, Clark Christopher, Hendry Aenea, Lerner Oleg, Hintze Mark, Allen James, Chilton John K., Guthrie Sarah (2012) **Axon guidance in the developing ocular motor system and duane retraction syndrome depends on semaphorin signaling via alpha2-chimaerin** *Proceedings of the National Academy of Sciences* **109**

118. Guthrie Sarah (2007) **Patterning and axon guidance of cranial motor neurons** *Nature Reviews Neuroscience* **8**

119. Peusner Kenna D., Morest D.K. (1977) **The neuronal architecture and topography of the nucleus vestibularis tangentialis in the late chick embryo** *Neuroscience* **2**:189–IN2

120. Ronca April E., French Alison J., Smith Jeffrey D. (2016) **Translating basic research to astronaut health in space: Nasa ames rodent specimen biobanking for the human research program** *Gravitational and Space Research* **4**

121. Riley Bruce B., Moorman Stephen J. (2000) **Development of utricular otoliths, but not saccular otoliths, is necessary for vestibular function and survival in zebrafish** *Journal of Neurobiology* **43**:329–337

122. Roberts Richard, Elsner Jeffrey, Bagnall Martha W. (2017) **Delayed otolith development does not impair vestibular circuit formation in zebrafish** *Journal of the Association for Research in Otolaryngology* **18**:415–425

123. Ulrich Florian, Grove Charlotte, Torres-Vázquez Jesús, Baker Robert (2014) **Development of functional hindbrain oculomotor circuitry independent of both vascularization and neuronal activity in larval zebrafish** *Current Neurobiology* **7**:62–73

124. Schindelin Johannes *et al.* (2012) **Fiji: an open-source platform for biological-image analysis** *Nature Methods* **9**:676–682

125. Caron S. J. C., Prober D., Choy M., Schier A. F. (2008) **In vivo birthdating by BAPTISM reveals that trigeminal sensory neuron diversity depends on early neurogenesis** *Development* **135**:3259–3269

126. Barsh Gabrielle R., Isabella Adam J., Moens Cecilia B. (2017) **Vagus motor neuron topographic map determined by parallel mechanisms of hox5 expression and time of axon initiation** *Current Biology* **27**:3812–3825

127. Ibarra-García-Padilla Rodrigo (2021) **Aubrey Gaylon Adam Howard, Eileen Willey Singleton, and Rosa Anna Uribe. A protocol for whole-mount immuno-coupled hybridization chain reaction (wichcr) in zebrafish embryos and larvae** *STAR Protocols* **2**

128. Kuehn Emily, Clausen David S., Null Ryan W., Metzger Bria M., Willis Amy D., Duygu Özpolat B. (2021) **Segment number threshold determines juvenile onset of germline cluster expansion in platynereis dumerilii** *Journal of Experimental Zoology Part B: Molecular and Developmental Evolution* **338**

129. Love Michael I, Huber Wolfgang, Anders Simon (2014) **Moderated estimation of fold change and dispersion for rna-seq data with deseq2** *Genome Biology* **15**

130. Pfaff Samuel L., Mendelsohn Monica, Stewart Colin L., Edlund Thomas, Jessell Thomas M. (1996) **Requirement for lim homeobox gene isl1 in motor neuron generation reveals a motor neuron dependent step in interneuron differentiation** *Cell* **84**

131. Tokumoto Mika, Gong Zhiyuan, Tsubokawa Tatsuya, Hew Choy L., Uyemura Keiichi, Hotta Yoshiki, Okamoto Hitoshi (1995) **Molecular heterogeneity among primary motoneurons and within myotomes revealed by the differential mrna expression of novel islet-1 homologs in embryonic zebrafish** *Developmental Biology* **171**

132. Prince Victoria E., Moens Cecilia B., Kimmel Charles B., Ho Robert K. (1998) **Zebrafish hox genes: expression in the hindbrain region of wild-type and mutants of the segmentation gene, valentino** *Development* **125**

133. Hao Yuhan *et al.* (2021) **Integrated analysis of multimodal single-cell data** *Cell* **184**:3573–3587

134. Efron B., Tibshirani R. (1986) **Bootstrap methods for standard errors, confidence intervals, and other measures of statistical accuracy** *Statistical Science* **1**:54–75

Article and author information

Dena Goldblatt
Depts. of Otolaryngology, Neuroscience & Physiology, and the Neuroscience Institute, NYU Langone Health, Center for Neural Science, New York University
ORCID iD: 0000-0003-0333-2433

Başak Rosti
Depts. of Otolaryngology, Neuroscience & Physiology, and the Neuroscience Institute, NYU Langone Health
ORCID iD: 0009-0008-9838-8272

Kyla R. Hamling
Depts. of Otolaryngology, Neuroscience & Physiology, and the Neuroscience Institute, NYU Langone Health
ORCID iD: 0000-0001-5408-9256

Paige Leary
Depts. of Otolaryngology, Neuroscience & Physiology, and the Neuroscience Institute, NYU Langone Health
ORCID iD: 0000-0002-0888-466X

Harsh Panchal
Depts. of Otolaryngology, Neuroscience & Physiology, and the Neuroscience Institute, NYU Langone Health

Marlyn Li
Depts. of Otolaryngology, Neuroscience & Physiology, and the Neuroscience Institute, NYU Langone Health, Center for Neural Science, New York University
ORCID iD: 0009-0008-2144-7756

Hannah Gelnaw
Depts. of Otolaryngology, Neuroscience & Physiology, and the Neuroscience Institute, NYU Langone Health
ORCID iD: 0000-0002-7970-796X

Stephanie Huang
Depts. of Otolaryngology, Neuroscience & Physiology, and the Neuroscience Institute, NYU Langone Health, Center for Neural Science, New York University
ORCID iD: 0009-0002-0609-1655

Cheryl Quainoo
Depts. of Otolaryngology, Neuroscience & Physiology, and the Neuroscience Institute, NYU Langone Health

David Schoppik
Depts. of Otolaryngology, Neuroscience & Physiology, and the Neuroscience Institute, NYU Langone Health
For correspondence: schoppik@gmail.com
ORCID iD: 0000-0001-7969-9632

Editors

Reviewing Editor
John Tuthill
University of Washington, Seattle, United States of America

Senior Editor
Albert Cardona
University of Cambridge, Cambridge, United Kingdom

Reviewer #1 (Public Review):

Summary:

This study has as its goal to determine how the structure and function of the circuit that stabilizes gaze in the larval zebrafish depends on the presence of the output cells, the motor neurons. A major model of neural circuit development posits that the wiring of neurons is instructed by their postsynaptic cells, transmitting signals retrogradely on which cells to contact and, by extension, where to project their axons. Goldblatt et al. remove the motor neurons from the circuit by generating null mutants for the phox2a gene. The study then shows that, in this mutant that lacks the isl1-labelled extraocular motor neurons, the central projection neurons have 1) largely normal responses to vestibular input; 2) normal gross morphology; 3) minimally changed transcriptional profiles. From this, the authors conclude that the wiring of the circuit is not instructed by the output neurons, refuting the major model.

Strengths:

I found the manuscript to be exceptionally well-written and presented, with clear and concise writing and effective figures that highlight key concepts. The topic of neural circuit wiring is central to neuroscience, and the paper's findings will interest researchers across the field, and especially those focused on motor systems.

The experiments conducted are clever and of a very high standard, and I liked the systematic progression of methods to assess the different potential effects of removing phox2a on circuit structure and function. Analyses (including statistics) are comprehensive and appropriate and show the authors are meticulous and balanced in most of the conclusions that they draw. Overall, the findings are interesting, and with a few tweaks, should leave little doubt about the paper's main conclusions.

Weaknesses:

The main point is the incomplete characterisation of the effects of removing phox2a on the extra-ocular motor neurons. Are these cells no longer there, or are they there but no longer labelled by isl1:GFP? If they are indeed removed, might they have developed early on, and subsequently lost? These questions matter as the central focus of the manuscript is whether

the presence of these cells influences the connectivity and function of their presynaptic projection neurons. Therefore, for the main conclusions to be fully supported by the data, the authors would need to test whether 1) the motor neurons that otherwise would have been labelled by the isl1:GFP line are physically no longer there; 2) that this removal (if, indeed, it is that) is developmental. If these experiments are not feasible, then the text should be adjusted to take this into account. A further point to address is the context of the manipulation. If the phox2a removal does indeed take out the extra-ocular motor neurons, what percentage of postsynaptic neurons to the projection neurons are still present? In other words, how does the postsynaptic nMLF output relate to the motor neurons? If, for instance, the nMLF (which, as the authors state, are likely still innervated by the projection neurons) are the main output of the projections neurons, then this would affect the interpretation of the results.

https://doi.org/10.7554/eLife.96893.1.sa2

Reviewer #2 (Public Review):

Summary:

This study was designed to test the hypothesis that motor neurons play a causal role in circuit assembly of the vestibulo-ocular reflex circuit, which is based on the retrograde model proposed by Hans Straka. This circuit consists of peripheral sensory neurons, central projection neurons, and motor neurons. The authors hypothesize that loss of extraocular motor neurons, through CRISPR/Cas9 mutagenesis of the phox2a gene, will disrupt sensory selectivity in presynaptic projection neurons if the retrograde model is correct.

Account of the major strengths and weaknesses of the methods and results:

The work presented is impressive in both breadth and depth, including the experimental paradigms. Overall, the main results were that the loss of function paradigm to eliminate extraocular motor neurons did not 1) alter the normal functional connections between peripheral sensory neurons and central projection neurons, 2) affect the position of central projection neurons in the sensorimotor circuit, or 3) significantly alter the transcriptional profiles of central projection neurons. Together, these results strongly indicate that retrograde signals from motor neurons are not required for the development of the sensorimotor architecture of the vestibulo-ocular circuit.

Appraisal of whether the authors achieved their aims, and whether the results support their conclusions:

The results of this study showed that extraocular motor neurons were not required for central projection neuron specification in the vestibulo-ocular circuit, which countered the prevailing retrograde hypothesis proposed for circuit assembly. A concern is that the results presented may be limited to this specific circuit and may not be generalizable to other circuit assemblies, even to other sensorimotor circuits.

Discussion of the likely impact of the work on the field, and the utility of the methods and data to the community:

As mentioned above, this study sheds valuable new insights into the developmental organization of the vestibulo-ocular circuit. However, different circuits likely utilize various mechanisms, extrinsic or intrinsic (or both), to establish proper functional connectivity. So, the results shown here, although begin to explain the developmental organization of the vestibulo-ocular circuit, are not likely to be generalizable to other circuits; though this remains to be seen. At a minimum, this study provides a starting point for the examination of patterning of connections in this and other sensorimotor circuits.

https://doi.org/10.7554/eLife.96893.1.sa1

Reviewer #3 (Public Review):

In this manuscript by Goldblatt et al. the authors study the development of a well-known sensorimotor system, the vestibulo-ocular reflex circuit, using Danio rerio as a model. The authors address whether motor neurons within this circuit are required to determine the identity, upstream connectivity and function of their presynaptic partners, central projection neurons. They approach this by generating a CRISPR-mediated knockout line for the transcription factor phox2a, which specifies the fate of extraocular muscle motor neurons. After showing that phox2a knockout ablates these motor neurons, the authors show that functionally, morphologically, and transcriptionally, projection neurons develop relatively normally.

Overall, the authors present a convincing argument for the dispensability of motor neurons in the wiring of this circuit, although their claims about the generalizability of their findings to other sensorimotor circuits should be tempered. The study is comprehensive and employs multiple methods to examine the function, connectivity and identity of projection neurons.

Specific comments:

(1) In the introduction the authors set up the controversy on whether or not motor neurons play an instructive role in determining "pre-motor fate". This statement is somewhat generic and a bit misleading as it is generally accepted that many aspects of interneuron identity are motor neuron-independent. The authors might want to expand on these studies and better define what they mean by "fate", as it is not clear whether the studies they are citing in support of this hypothesis actually make that claim.

(2) Although it appears unchanged from their images, the authors do not explicitly quantitate the number of total projection neurons in phox2a knockouts.

(3) For figures 2C and 3C, please report the proportion of neurons in each animal, either showing individual data points here or in a separate supplementary figure; and please perform and report the results of an appropriate statistical test.

(4) In the topographical mapping of calcium responses (figures 2D, E and 3D), the authors say they see no differences but this is hard to appreciate based on the 3D plotting of the data. Quantitating the strength of the responses across the 3-axes shown individually and including statistical analyses would help make this point, especially since the plots look somewhat qualitatively different.

(5) The transcriptional analysis is very interesting, however, it is not clear why it was performed at 72 hpf, while functional experiments were performed at 5 days. Is it possible that early aspects of projection neuron identity are preserved, while motor neuron-dependent changes occur later? The authors should better justify and discuss their choice of timepoint. The inclusion of heterozygotes as controls is problematic, given that the authors show there are notable differences between phox2a+/+ and phox2a+/- animals; pooling these two genotypes could potentially flatten differences between controls and phox2a-/-.

(6) Projection neurons appear to be topographically organized and this organization is maintained in the absence of motor neurons. Are there specific genes that delineate ventral and dorsal projection neurons? If so, the authors should look at those as candidate genes as they might be selectively involved in connectivity. Showing that generic synaptic markers (Figure 4E) are maintained in the entire population is not convincing evidence that these neurons would choose the correct synaptic partners.

https://doi.org/10.7554/eLife.96893.1.sa0